



Paleomagnetism of a Neoproterozoic–Paleoproterozoic carbonate ramp and carbonate platform succession (Transvaal Supergroup) from surface outcrop and drill core, Griqualand West region, South Africa

M.O. de Kock^{a,c,*}, D.A.D. Evans^a, J.L. Kirschvink^b, N.J. Beukes^c, E. Rose^a, I. Hilburn^b

^a Department of Geology and Geophysics, Yale University, New Haven, CT, USA

^b Division of Geological and Planetary Sciences, California Institute of Technology, Pasadena, CA, USA

^c Paleoproterozoic Mineralization Research Group, University of Johannesburg, Auckland Park 2006, South Africa

ARTICLE INFO

Article history:

Received 24 December 2007

Received in revised form 12 May 2008

Accepted 23 October 2008

Keywords:

Paleomagnetism

Paleoproterozoic

South Africa

Apparent polar wander path

Remagnetization

Epigenetic mineralization

ABSTRACT

Detailed paleomagnetic study across the Archean–Paleoproterozoic boundary interval preserved in the Ghaap Group, Transvaal Supergroup, of the Kaapvaal craton reveals a complex series of viscous and thermo-chemical magnetic overprints. Despite this complex history, a potential primary single-polarity remanence direction was revealed at high-temperature demagnetization steps in about 10% of orientated drill core samples only. This component (declination = 132°, inclination = 69°) was not identified in any of the outcrop sites. Overprint directions include a present geomagnetic field remanence and a very well developed thermo-chemical overprint (declination = 359°, inclination = 54°), which is believed to be associated with a ~2.0 Ga regional thermal event and the development of extensive epigenetic Pb–Zn deposits. At higher levels of demagnetization, two shallow west-directed components appear to be related to the extrusion of the Ongeluk Formation lava at 2.22 Ga (declination = 268°, inclination = –20°; eastern parts of the studied region) and to the post-1.92 Ga Kheis orogeny (declination = 272°, inclination = 16°; exclusive to the western margin of the study area), respectively.

© 2008 Elsevier B.V. All rights reserved.

1. Introduction

The Agouron–Griqualand Paleoproterozoic Drilling Project was initiated to study the Archean–Paleoproterozoic transition recorded within the Transvaal Supergroup, western South Africa (Fig. 1). Drilling initially focussed on deepwater and slope facies (boreholes GKP1 and GKF1) of the lower Transvaal Supergroup, to further understanding of the paleoenvironmental changes across the shelf to basin transition. Even though the Neoproterozoic–Paleoproterozoic interval is well studied in South Africa, and a sound understanding exists of the sequence stratigraphic framework in which the lower Transvaal Supergroup developed (e.g., Sumner and Beukes, 2006), the first two Agouron cores fill a gap that is not well represented in outcrop (Fig. 1).

The goals of this paper are threefold. First, we aim to provide paleolatitude constraints on this key stratigraphic record by determining reliable Archean–Paleoproterozoic paleopoles from core and outcrop sampling. Secondly, we aim to construct a magnetostratigraphy to aid correlation between drill core and outcrop. Finally, this study can help to assess the degree of thermochemical alteration within these rocks, and constrain the nature and timing of hydrothermal fluids potentially responsible for resetting geochemical and isotopic records.

* Corresponding author at: Paleoproterozoic Mineralization Research Group, University of Johannesburg, Auckland Park 2006, South Africa. Tel.: +27 11 559 2301; fax: +27 11 559 2309.

E-mail address: mdekock@uj.ac.za (M.O. de Kock).

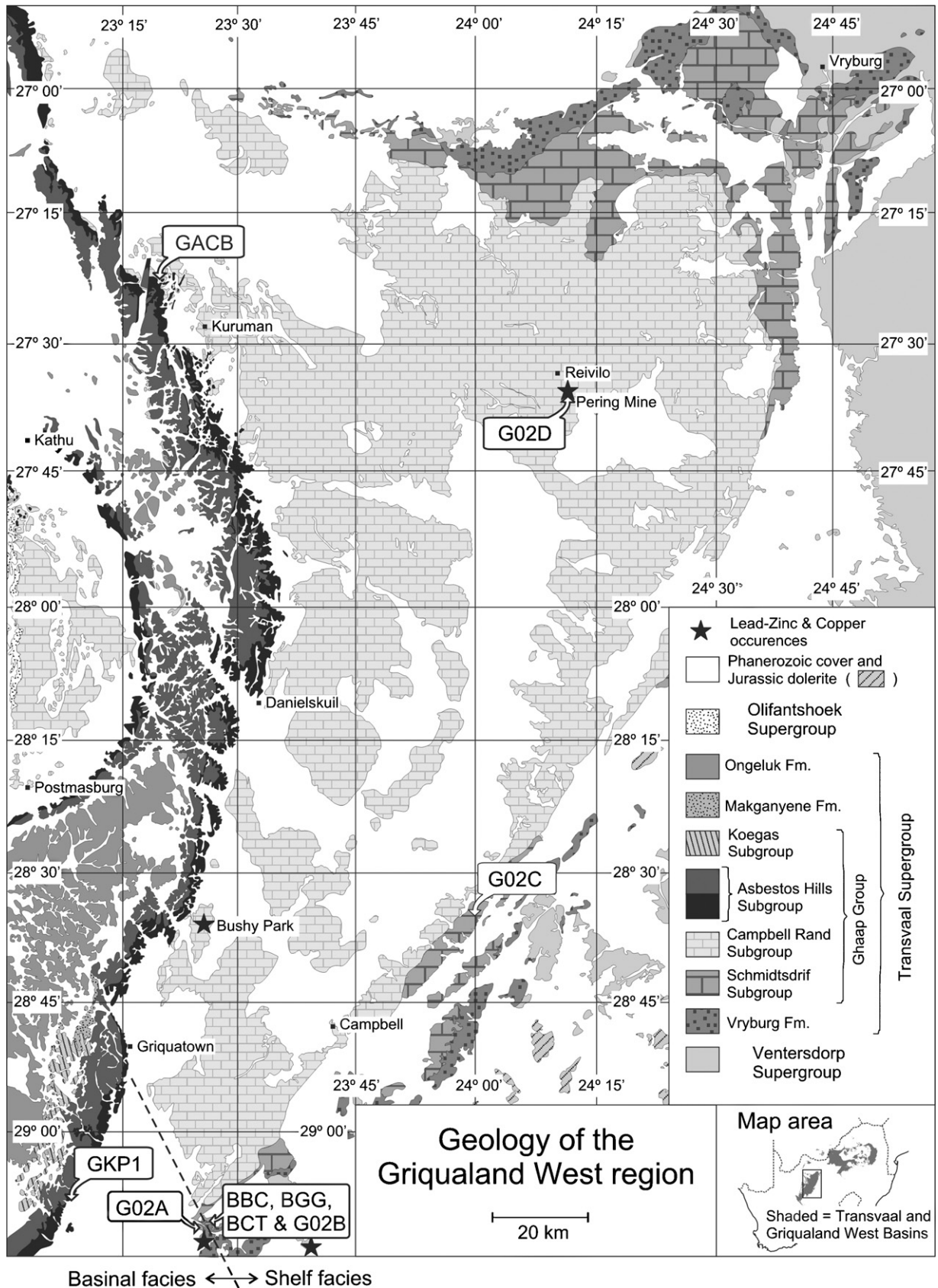


Fig. 1. Geology of the Griqualand West region displaying the location of paleomagnetic sampling sites for this study as well as the location of drill core GKP1.

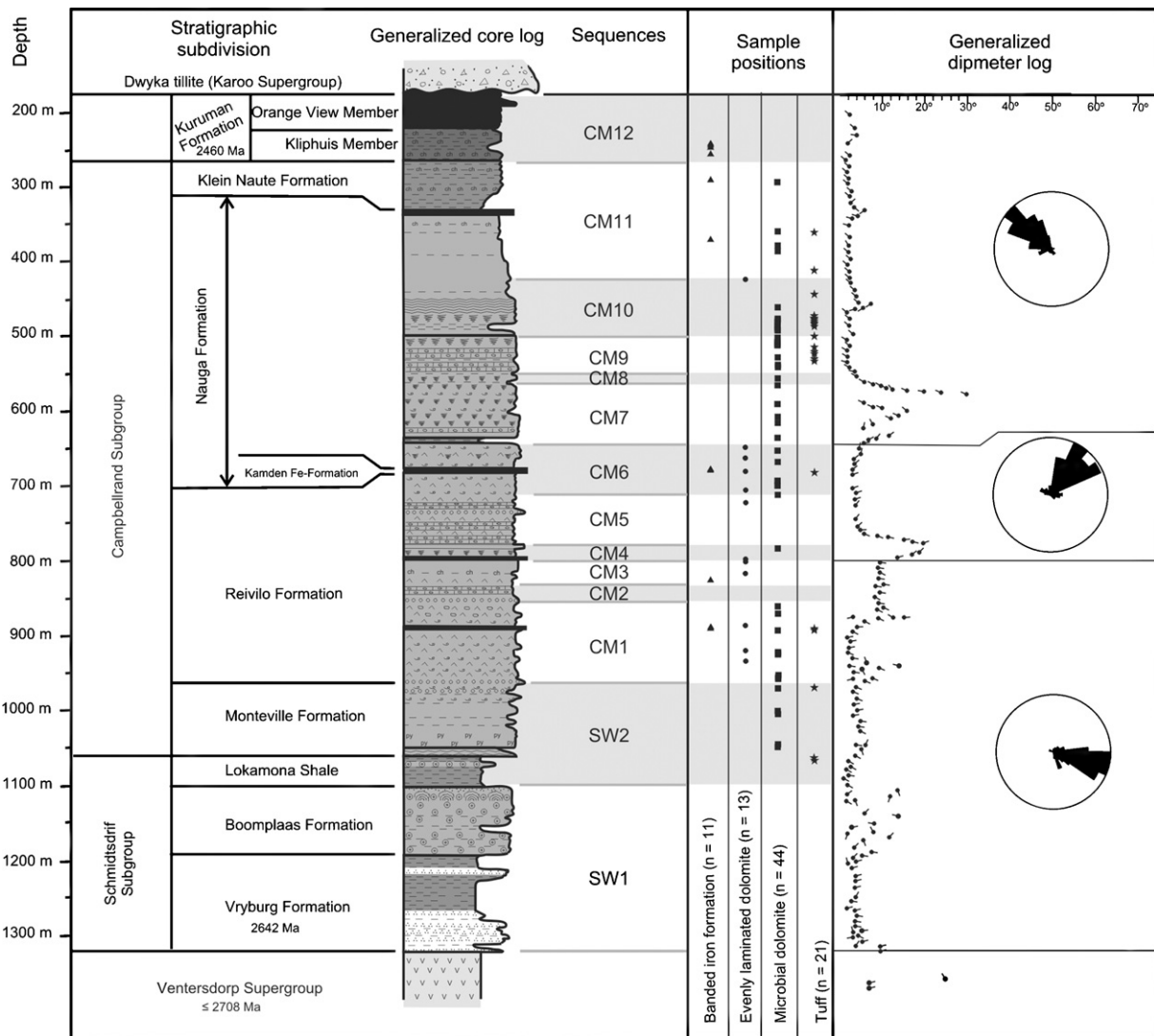


Fig. 2. Generalized stratigraphic log of drill core GKP1. Sequence-stratigraphic subdivision following Sumner and Beukes (2006) is indicated. The Schmidtsdrif-Wolkberg sequences, or SW1 and SW2, represent the development of the lower Transvaal mixed siliciclastic-carbonate ramp after the extrusion of the Ventersdorp Supergroup basalts. The first Campbellrand-Malmani sequence, or CM1, represents a craton-wide transgression and CM2-5 represents the development of a steep platform margin. A transgression deep into the interior of the craton is marked by sequence CM6, while sequences CM7-11 record the development of lagoons and a high-relief margin. The carbonate platform was ultimately drowned and extensive banded-iron formations were deposited (CM12). Paleomagnetic sample positions and their lithologies are indicated. The generalized dip-meter log shows that strata have shallow dips throughout the depth of the core and only have experienced slight structural warping.

bellrand and Asbestos Hills Subgroups) were recently reviewed by Schröder et al. (2006) in their description of the first of the Agouron cores—GKP1. The Schmidtsdrif Subgroup is a mixed siliciclastic-carbonate ramp succession deposited between 2664 ± 6 and 2642 ± 3 Ma (Barton et al., 1995; Walraven and Martini, 1995) and is conformably overlain by the Campbellrand/Malmani succession. The Campbellrand/Malmani succession represents two laterally equivalent carbonate sequences (Beukes, 1987)—a thin basal deepwater succession to the southwest off the edge of the craton in Griqualand West, and a relatively thick continental shelf succession deposited in shallower water on the craton in both the Griqualand West and Transvaal regions. In contrast to the predominantly stromatolitic shallow shelf sequence (Beukes, 1987; Sumner, 1997; Sumner and Grotzinger, 2004), the basal sequence is made up of microbialitic, finely laminated carbonates and siliciclastic mudstone, chert and thin beds of iron formation—the so-called Prieska Facies. Chert and banded-iron formation of the Asbestos Hills Subgroup conformably overlie the Campbellrand Subgroup, representing drowning of the platform at about 2.5 Ga (Pickard,

2003; Sumner and Bowring, 1996). Borehole GKP1 (Fig. 2) provides a complete record of the basal carbonate ramp (i.e., Schmidtsdrif Subgroup) as well as the distal slope equivalent facies of the carbonate platform development and drowning episode (14 sequences described by Sumner and Beukes, 2006).

In principle, the Transvaal Supergroup should lend itself well to paleomagnetic study. Most outcrops have only experienced lower greenschist facies metamorphism (Button, 1973; Miyano and Beukes, 1984), and amphibolite facies is only reached in proximity to the ~ 2.06 -Ga old (Buick et al., 2001; Walraven, 1997; Walraven and Hattingh, 1993) Bushveld Complex. Supergene alteration associated with late fluid flow coeval with the Bushveld Complex (Duane et al., 2004), but not necessarily related to its intrusion, is responsible for Pb-Zn mineralization developed at various localities within the Campbellrand and Malmani Subgroups (Duane et al., 2004; Greyling et al., 2001; Gutzmer, 2006; Huizenga et al., 2006a,b). Hydrothermal gold and fluoride mineralization of an unknown age have also been reported (e.g., Button, 1979).

3. Sampling and method

3.1. Outcrops

We sampled limestone and shale of the Schmidtsdrif Subgroup (i.e., the Boomplaas and Monteville Formations) and limestone from the Cambellrand Subgroup at the now abandoned Pering Pb–Zn Mine and from a locality close to Kuruman (Gamohaana) in northern Griqualand West (Fig. 1). The outcrop sampling permits paleomagnetic field stability tests (i.e., conglomerate tests on micritic limestone intraclasts in a sedimentary breccia within the Boomplaas Formation and a baked contact test between lithologies of the Boomplaas Formation and an undated N–S trending dolerite dyke), which could not be achieved for the drill core. Samples were drilled with a portable, hand-held petrol drill. Orientation was achieved by magnetic compass, and for most samples also a sun compass.

3.2. Drill core

The GKP1 borehole was inclined at a 15° angle from vertical in the direction of the surface dip of the strata, which did not exceed 5°. This maximised the ellipticity of bedding intersections, aiding azimuthal orientations. Borehole control was maintained throughout drilling, and the retrieved core was left on the topside with an impact “ballmark” alongside the drilling azimuth. Wireline tools run after drilling further assisted in the orientation of paleomagnetic samples.

Retrieved core was halved along its azimuth axis, and the northern half was sampled (Fig. 2). All sequences from the Lokamona shale upward to the base of the Kuruman Iron Formation are represented. Sampling involved drilling small cylindrical core specimens (2.5-cm diameter) perpendicular to the flat cut (south-facing) sides of the halved drill cores, thus yielding specimens with zero plunge. Specimen strike was taken as 180° from the borehole azimuth at each specific sampling depth. Specimens were trimmed to ~2 cm height. The sampled half of the core is archived at the Smithsonian Institution, Washington, DC whereas the other half is stored at the Council for Geosciences in Pretoria, South Africa.

3.3. Laboratory

Trimmed specimens were measured on 2G Enterprises™ SQUID magnetometers equipped with automatic sample-changing systems (Kirschvink et al., 2008) at the California Institute of Technology and Yale University. Demagnetization generally consisted of 15–40 steps. Outcrop samples were typically pre-treated with low-field-strength alternating-field (AF) demagnetization up to 20 mT, then thermally demagnetized in a magnetically shielded furnace from 100 to 510 °C. For some sites thermal demagnetization up to 360 °C was followed by high-field AF demagnetization from 40 to 70 mT.

After being grouped by lithology, drill core samples were pre-treated with AF demagnetization up to 10 mT, then thermally demagnetized from 100 to 500 °C in 15–20 steps at decreasing intervals or until specimen intensity dropped below noise level. The demagnetization procedure (temperature interval, size, etc.) varied greatly according to lithology.

Magnetic components were identified via least-squares analysis (Kirschvink, 1980). Fits with error angles $\leq 15^\circ$ were used to calculate directional means, and only means with α_{95} and k -parameter values of $\leq 15^\circ$ and ≥ 10 , respectively were used to calculate virtual geomagnetic poles (VGPs). Calculations and all subsequent statistical analyses utilized the software Paleomag (Jones, 2002) and Paleomac (Cogné, 2003).

4. Results

4.1. Outcrops

Four magnetic components were identified (see Table 1 at the end of Section 4), three of which can convincingly shown to be younger overprints. A field stability test could not be performed for the fourth component, but it too is believed to be a younger remanence.

4.1.1. Boomplaas Formation (Sequence SW1)

The Boomplaas Formation crops out along a narrow gorge cut by the Orange River in the southern Griqualand West region, accessed from Gewonne farm. We sampled five sites, including two intraformational conglomerate tests and one baked-contact test (Fig. 3).

Sample demagnetization behaviour fell into two groups. In the first group, sample remanence is dominated by single uniformly (“randomly”) distributed components (e.g., BBC 5.1, Fig. 4(a)). These magnetizations exhibit behaviour uncharacteristic of lightning induced magnetizations, being readily demagnetized by the AF method, and displaying humped patterns on J/J_{\max} diagrams (e.g., BBC 5.1, Fig. 4(a)). Samples may instead suffer from limitations imposed by the grain size of their magnetic minerals. Thirty to 40% of samples from site G02A 1–28 and site BCC display this enigmatic behaviour (Fig. 5).

In the second group, beneath the unstable magnetic components removed by low-field AF demagnetization, samples record three stable components. The first component (Present Earth Field, abbreviated PEF) unblocks at temperatures up to 250 °C, and has a northerly and upward direction similar to the axial dipole field. A second component is northerly and downward directed (ND) and unblocks between 250 and 320–380 °C. In many samples from site G02A, the ND component does not decay towards the origin of the demagnetization plot (Fig. 4(b) and (c)), but further demagnetization does not reveal any stable underlying component. In contrast, thermal demagnetization above 320–380 °C in samples from site BBC and BGG reveals a third component with a shallow westerly direction (Fig. 4(a) and (c)). Linear fits for this component dominantly have shallow downward inclinations (W+; e.g., BBC 3.1 in Fig. 4(a)), but in a few cases inclinations are upward directed (W–; e.g., BGG 5 in Fig. 4(c)). The W– components were grouped with the W+ components for the calculation of directional means (Fig. 5). This may result in the mixing of two distinct components, but excluding the W– components does not significantly alter the

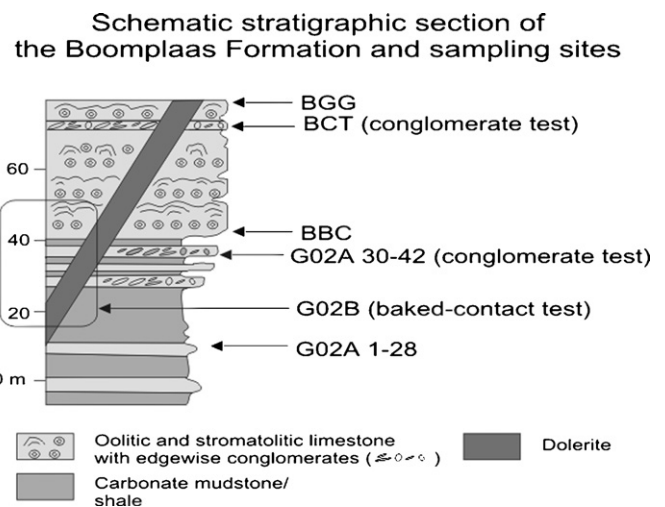


Fig. 3. Schematic stratigraphic section of the Boomplaas Formation and sampling sites at Gewonne Gorge.

Table 1
Summary of least-squares component directions for the Ghaap Group from outcrop and drill core.^a

COMPONENT in boldface Sequence (Fm.)	Site	Lithology	<i>n/N</i>	<i>L/P</i>	Max. Unbl.	Present coordinates				Tectonically-corrected coordinates			
						<i>D</i> in deg.	<i>I</i> in deg.	<i>k</i>	α_{95} in deg.	<i>D</i> in deg.	<i>I</i> in deg.	<i>k</i>	α_{95} in deg.
Secondary components constrained by field tests													
PEF													
SW1 (Boomplaas Fm.)	<u>G02A</u>	Micritic limestone	17/25	17/0	250 °C	<u>350.9</u>	<u>-47.2</u>	<u>25.1</u>	<u>7.3</u>	350.9	-47.2	25.1	7.3
	<u>G02A</u> (congl.)	Micritic intraclasts	16/18	16/0	250 °C	<u>333.2</u>	<u>-57.5</u>	<u>16.0</u>	<u>9.5</u>	330.1	-36.3	5.0	18.3
	BBC	Stromatolitic limestone and dolomite	2/5	2/0	250 °C	317.5	-57.9	-	-	317.5	-57.9	-	-
	<u>G02B</u>	Stromatolitic limestone shale, hornfels and dolerite	20/52	20/0	~250 °C	<u>356.1</u>	<u>-47.1</u>	<u>11.8</u>	<u>9.9</u>	353.8	-47.4	12.5	9.6
	<u>BCT</u> (congl.)	Edgewise conglomerate	11/11	11/0	250 °C	<u>328.8</u>	<u>-46.3</u>	<u>33.8</u>	<u>7.6</u>	332.0	-49.1	33.8	7.6
	<u>BGG</u>	Stromatolitic limestone and carbonate sst.	9/13	9/0	250 °C	<u>328.7</u>	<u>-50.5</u>	<u>14.8</u>	<u>13.0</u>	331.9	-53.3	14.6	13.1
SW2 (Monteville Fm.)	<u>G02C</u>	Shale and limestone	20/21	20/0	225–275 °C	<u>343.6</u>	<u>-53.0</u>	<u>49.2</u>	<u>4.7</u>	340.6	-53.3	43.6	5.0
CM5 (Reivilo Fm.)	<u>G02D</u>	Dark grey limestone (partly mineralized)	17/20	17/0	225–250 °C	<u>339.2</u>	<u>-45.5</u>	<u>100.6</u>	<u>3.6</u>	333.2	-40.1	9.6	12.1
CM11 (Gamohaam Fm.)	GACB	Limestone	5/7	5/0	250 °C	336.4	-45.5	6.7	28.0	337.4	-47.3	6.7	28.2
SW1-CM12 (Boomplaas to Kuruman Fm.)	GKP1	Microbially-laminated carbonate, evenly-laminated carbonate, tuff and banded-iron formation	37/87	37/0	240 °C	322.4	-57.8	12.1	7.1	324.2	-67.7	12.9	6.8
ND													
SW1 (Boomplaas Fm.)	G02A	Micritic limestone	15/25	15/0	~380 °C	345.8	44.8	9.3	13.8	345.8	44.8	9.3	13.8
	<u>G02A</u> (congl.)	Micritic intraclasts	16/18	16/0	380 °C	<u>2.1</u>	<u>47.9</u>	<u>161.5</u>	<u>2.1</u>	26.9	55.3	6.3	15.9
	BBC	Stromatolitic limestone and dolomite	3/5	3/0	~380 °C	<u>349.1</u>	<u>63.2</u>	<u>84.5</u>	<u>11.0</u>	349.1	63.2	84.5	11.0
	G02B	Stromatolitic limestone shale, hornfels and dolerite	30/52	30/0	360 °C	13.6	45.1	9.9	8.8	14.8	44.5	9.7	8.9
	<u>BCT</u> (congl.)	Edgewise conglomerate	11/11	11/0	380 °C	<u>10.6</u>	<u>54.3</u>	<u>253.4</u>	<u>2.7</u>	5.1	53.9	252.8	2.7
	<u>BGG</u>	Stromatolitic limestone and carbonate sst.	12/13	12/0	320–380 °C	<u>16.9</u>	<u>56.4</u>	<u>121.8</u>	<u>3.8</u>	16.9	56.4	121.8	3.8
SW2 (Monteville Fm.)	<u>G02C</u>	Shale and limestone	18/21	18/0	380 °C	<u>6.8</u>	<u>48.4</u>	<u>85.3</u>	<u>3.8</u>	11.3	49.8	81.2	3.9
CM5 (Reivilo Fm.)	<u>G02D</u>	Dark grey limestone (partly mineralized)	19/20	19/0	380 °C	<u>357.6</u>	<u>54.4</u>	<u>280.3</u>	<u>2.8</u>	8.4	56.1	13.9	9.3
CM11 (Gamohaam Fm.)	GACB	Limestone	7/7	7/0	380 °C	<u>349.0</u>	<u>50.0</u>	<u>29.1</u>	<u>10.5</u>	347.3	48.6	29.0	10.5
SW1-CM12 (Boomplaas to Kuruman Fm.)	GKP1	Microbially-laminated carbonate, evenly-laminated carbonate, tuff and banded-iron formation	36/87	36/0	270–300 °C	<u>354.9</u>	<u>61.1</u>	<u>25.3</u>	<u>4.8</u>	348.6	55.3	20.2	5.4
W+													
SW1 (Boomplaas Fm.)	<u>G02A</u> (congl.)	Micritic intraclasts	15/18	15/0	440 °C	<u>262.3</u>	<u>21.3</u>	<u>34.8</u>	<u>6.3</u>	249.1	31.9	9.4	12.7
	BBC	Stromatolitic limestone and dolomite	2/5	1/1	510 °C	-	-	-	-	-	-	-	-
	G02B	Stromatolitic limestone and dolerite (Hornfels excluded)	8/45	6/4	65 mT	294.7	18.3	11.3	17.2	294.7	18.3	11.3	17.2

Table 1 (Continued)

COMPONENT in boldface Sequence (Fm.)	Site	Lithology	n/N	L/P	Max. Unbl.	Present coordinates				Tectonically-corrected coordinates			
						D in deg.	I in deg.	k	α_{95} in deg.	D in deg.	I in deg.	k	α_{95} in deg.
CM11 (Gamohaam Fm.)	<u>BCT</u> (congl.)	Edgewise conglomerate	10/11	8/2	440 °C	<u>272.1</u>	<u>15.7</u>	<u>18.4</u>	<u>12.4</u>	273.3	11.8	18.4	12.4
	<u>BGG</u>	Stromatolitic limestone and carbonate sst.	12/13	12/0	410 °C	<u>272.6</u>	<u>8.4</u>	<u>17.8</u>	<u>12.2</u>	272.6	8.4	17.8	12.2
	<u>GACB</u>	Limestone	7/7	4/3	470 °C	<u>282.4</u>	<u>17.2</u>	<u>27.4</u>	<u>14.9</u>	282.6	15.3	27.4	14.9
SW1-CM12 (Boomplaas to Kuruman Fm.)	GKP1	Microbially-laminated carbonate, evenly-laminated carbonate, tuff and banded-iron formation	2/87	2/0	440 °C	307.8	18.9	–	–	307.7	12.4	–	–
Components unconstrained by field tests													
LOW													
SW1-CM12 (Boomplaas to Kuruman Fm.)	GKP1	Microbially-laminated carbonate, evenly-laminated carbonate, tuff and banded-iron formation	33/87	33/0	10 mT	67.8	–77.6	74.4	2.9	91.8	–73.2	51.3	3.5
W+/-													
SW1 (Boomplaas Fm.)	G02B	Honfels only	7/7	7/0	65 mT	272.8	–0.8	85.8	6.6	272.8	–0.8	85.8	6.6
W-													
SW2 (Monteville Fm.)	<u>G02C</u>	Shale and limestone	14/21	11/3	470 °C	271.6	–19.6	24.1	8.8	<u>271.9</u>	<u>–16.8</u>	<u>24.3</u>	<u>8.8</u>
CM5 (Reivilo Fm.)	<u>G02D</u>	Dark grey limestone (partly mineralized)	18/20	18/0	490 °C	264.7	–20.4	278.7	2.1	<u>264.7</u>	<u>–20.4</u>	<u>278.7</u>	<u>2.1</u>
SD													
SW1-CM12 (Boomplaas to Kuruman Fm.)	<u>GKP1</u>	Microbially-laminated carbonate, evenly-laminated carbonate, tuff and banded-iron formation	10/87	10/0	470 °C	132.2	69.0	23.6	10.2	<u>135.2</u>	<u>77.6</u>	<u>20.2</u>	<u>11.0</u>

Underlined entries were not included for component-mean and paleomagnetic pole calculations.

^a Abbreviations: Fm. = Formation, n/N = number of samples included of total taken at specific site, L/P = number of linear fits vs. plane fits, Max. Unbl. = maximum temperature in °C or field-strength in mT at which component unblocks, D = declination, I = inclination, deg. = degrees, k = Fisher's (1953) precision parameter, α_{95} = radius of 95% confidence cone about the mean.

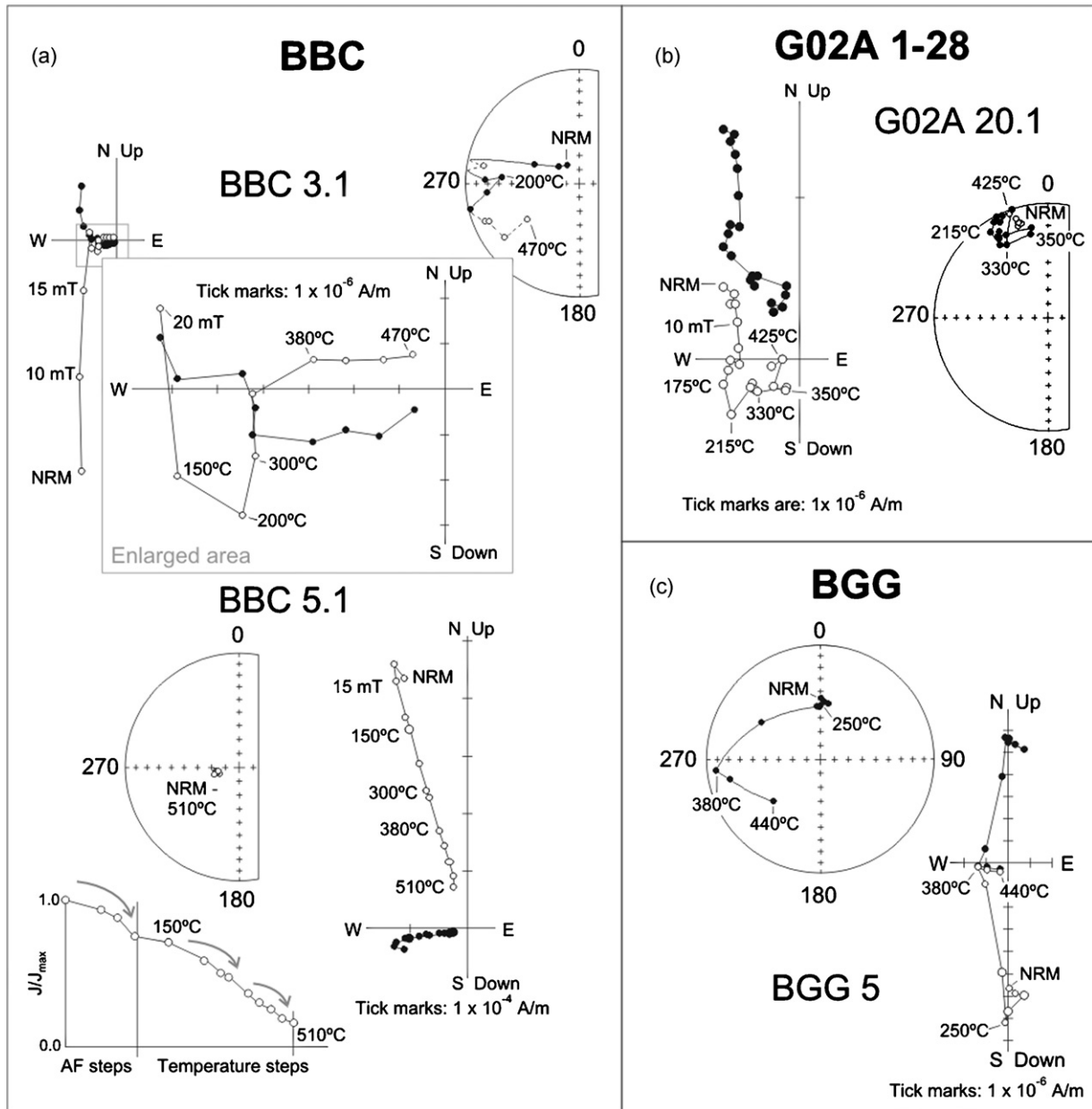


Fig. 4. Representative sample behaviour during demagnetization for essentially horizontal limestone and shale of the Boomplaas Formation. (a) Demagnetization of stromatolitic limestone from site BBC yielded three stable magnetizations, identifiable as linear fits in BBC 3.1, or anomalous single linear components, ex. BBC 5.1. Plots of normalized magnetization (J/J_{\max}) and demagnetization steps reveal behaviour unlike that expected of lightning induced isothermal remanent magnetizations. In sample BBC 3.1 a present geomagnetic field-like remanence was removed at 200 °C, after AF-pretreatment removed a low-coercivity component (coded PEF). Between 200 and 380 °C a northwesterly and down (ND) component was removed, while higher temperature steps to 470 °C revealed a shallow westerly component (W+). (b) Similar components were identified in samples from G02A with various degrees of success. (c) Limestone samples from site BGG were very consistent during demagnetization, yielding three readily identifiable components (PEF, ND and W+). Orthogonal plots: solid symbols = horizontal plane, open symbols = N–S and vertical plane. Equal area plots: solid symbols = lower hemisphere, open symbols = upper hemisphere.

calculated means. The W+/- components did not always decay towards the origin, which suggests that there may be an unresolved “harder” component of NRM, which is obscured by inconsistent demagnetization behaviour above 440 °C. In two samples from site BGG (e.g., BGG 5 in Fig. 4(c)) high-temperature demagnetization steps hint at a southerly and downward character for this obscured component, but no significant mean could be calculated.

4.1.1.1. Conglomerate tests. Intraclasts of micritic limestone from two sites, G02A 30–42 and BCT, respond well to demagnetization and three components were readily identified (Fig. 6(a) and (b)). Without applying any tilt-corrections to the clasts, these components are tightly clustered and mostly align with the PEF, ND and

W+ components discussed above (Fig. 6(c) and (d)), suggesting that these components post-date conglomerate formation. Bedding was measurable within most clasts from site G02A, allowing restoration back to paleohorizontal. This correction results in a wide range of inclinations for all three of the identified components (Fig. 6(c))—it fails the conglomerate test. Individual clast orientations from site BCT were not recorded.

Two clasts from the same core (G02A 41A and 41B, Fig. 6(c)) also record three components, but although the first component is PEF-like, confirming that the core was oriented correctly, the remaining two components are offset from one another as well as the components identified in the other clasts. The inconsistent directions at higher demagnetization levels are most likely due to component

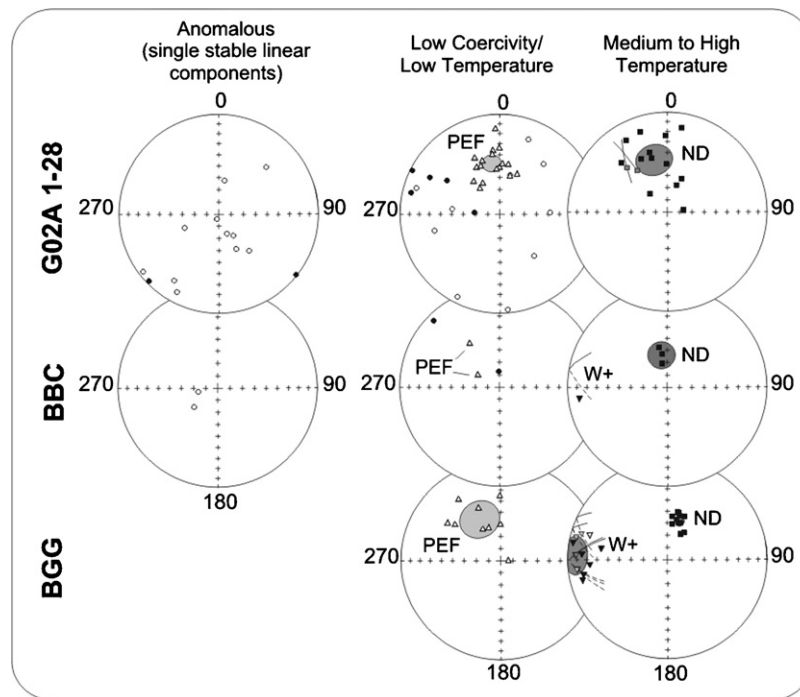


Fig. 5. Equal-area plots of remanence components from outcrop sites within the Boomplaas Formation in geographic coordinates. Open/lightly shaded symbols = upper hemisphere, closed/heavily shaded symbols = lower hemisphere. Shaded symbols on planes = planar fits, circles = low coercivity or anomalous component linear fits, upright triangles = PEF component linear fits, squares = ND component linear fits, downward triangles = W+ component linear fits. Shaded ellipses are component means and their associated 95% cones of confidence.

mixing, but potentially this sample, and the two clasts it contains, escaped remagnetization.

The stability of magnetization and overall good demagnetization behaviour sets apart the G02A conglomerate samples (30–42) from those taken lower in the succession (samples 1–28), being much more like that of samples from site BGG. The two conglomerate test sites and site BGG lie approximately along strike of a prominent west-northwesterly erosional lineament, which probably represents a fracture or fault (Fig. 6). Proximity to this lineament may have ensured sufficient interaction with a remagnetizing fluid.

4.1.1.2. Baked-contact test. A coarse- to medium-grained, ca. 100 m thick, dolerite dyke of unknown age intrudes the Boomplaas Formation, causing the usually sub-horizontal northwest dipping strata to be turned upwards (Fig. 7). We sampled within the baked contact zone, 1.2–1.9 m from the intrusion, and from progressively less-baked limestone (4–50 m away). An additional six shale samples were collected >100 m away from the dyke.

Coarse-grained dolerite from the centre of the intrusion is magnetically unstable, with single, “randomly” directed components that decay toward the origin. Closer to the contact, as the dolerite becomes finer-grained, more sense can be made of samples’ decay (Fig. 7 right and Fig. 8). After the removal of minor low-coercivity or “soft” NRM components, a present geomagnetic field-like (PEF) component unblocks. The so-called soft components are generally uniformly directed, but in four samples (G02B 9–12, Fig. 8) they cluster about a steep upward easterly direction, which is not observed in any of the other samples. The PEF mean is very poorly clustered ($k=4.7$). A northerly downward (ND) component then unblocks up to temperatures of about 315 °C. Although similar to the ND component identified at the other sites, the dolerite ND components are significantly scattered and the distribution is streaked towards the north. In a few samples (9–12, but the fit for sample 12 has an error of 15° so is not included in calculations) demagnetization follows a great circle arc trajectory away from shallow northerly directions towards a very steep north and up

direction (NU), which forms a stable end-point of thermal demagnetization between 315 and 360 °C. The ND and higher stability NU components may not be successfully separated by demagnetization in most of the samples, causing the observed streaking of the ND components. Unblocking spectra suggest that the NU component is carried by a magnetic phase with higher coercivity than pyrrhotite, presumably magnetite. Thermal demagnetization to 360 °C was followed with high-field-strength AF demagnetization from 40 to 70 mT. In five of the samples this resulted in an immediate “jump” of magnetization vectors away from the position of the last thermal step (usually around the ND component, the NU component or a mixture of those two) towards a shallow west and down direction (W+). In the other seven samples a similar jump was observed, but the resulting directions are scattered. The final high-level AF steps that describe the W+ components appear more scattered when viewed in specimen coordinates, bolstering our interpretation that a W+ remanence is recorded in some of the medium-grained dolerite samples. Unfortunately, the component mean is too poorly defined to be used in further calculations or comparisons.

Hornfels samples 16–22 from within the baked-contact zone, less than 2 m away from the intrusion are dominated by a shallow westerly characteristic remanence (Fig. 7), although three components are readily identifiable. The first two components are clearly PEF and ND components as seen elsewhere, while the third component unblocks as a nearly horizontal west-directed line that decays toward zero with high-field-strength AF steps. The mean of the westerly components is well defined and directed slightly upward (W–), which contrasts with the westerly down (W+) magnetizations identified elsewhere (Fig. 8). Since chemical and/or thermal remagnetization of the country rock is expected to be total at the contact with an intrusion, and since the fine-grained hornfels is probably a better magnetic recorder than medium-grained dolerite, we interpret the west-up (W–) remanence to be equivalent to the intrusion’s primary thermo-remanent magnetization.

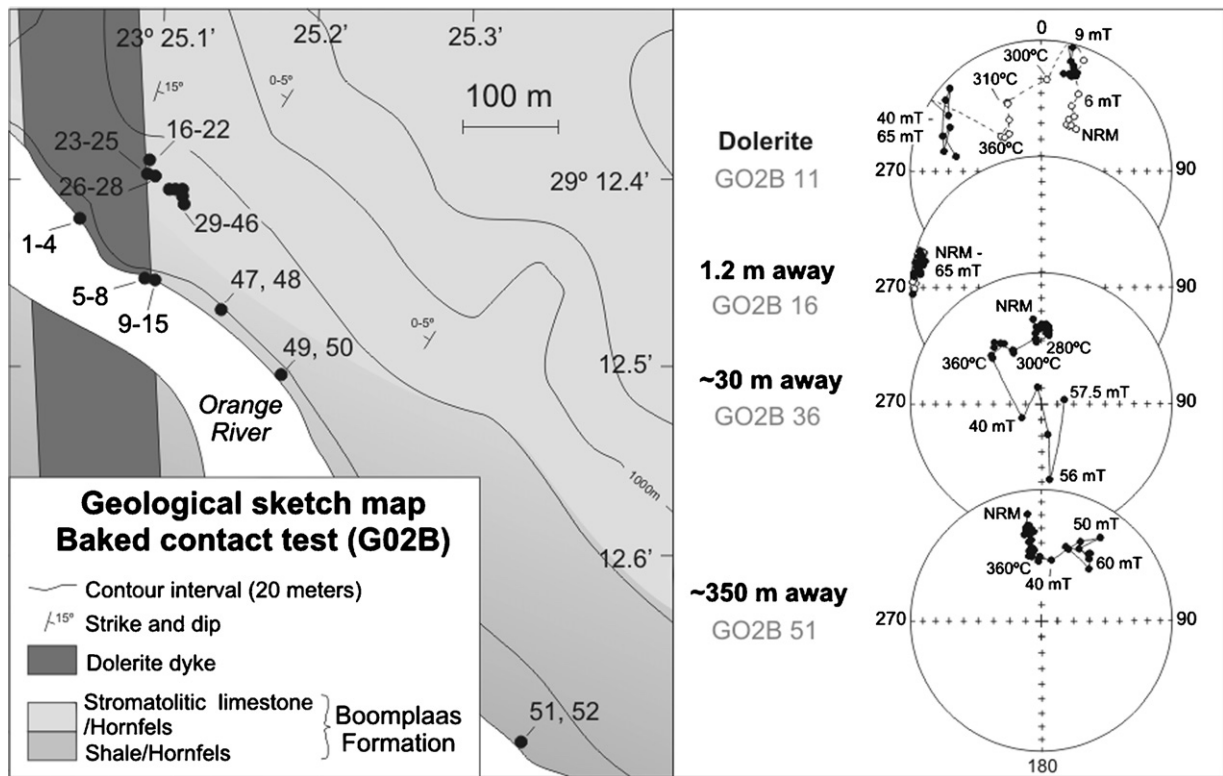


Fig. 7. Geological sketch map of the baked-contact test at site G02B and equal-area plots of sample demagnetization progressively farther away from the intrusion.

horizontal (W–) remanence of the hornfels is indeed different from the regionally present W+ direction, but formal comparison shows that the hornfels W– components are statistically indistinguishable from the W+ components from site BGG. The baked-contact test is therefore inconclusive.

4.1.1.3. Summary of components identified in the Boomplaas Formation. Four magnetic components were identified within the Boomplaas Formation. The first to unblock is a viscous remanence paralleling the present geomagnetic field (PEF), the second (ND) is believed to be carried by pyrrhotite and the third (W+) is revealed at higher levels of demagnetization. Samples originating from within a contact zone to a 100 m thick dolerite dyke displayed well-grouped near-horizontal westerly components at higher levels of demagnetization (W–). Conglomerate tests indicate the PEF, ND and W+ components are all later magnetic overprints. Although a baked-contact test is statistically inconclusive, we interpret the W– component as a thermal remanence associated with the dolerite intrusion.

4.1.2. Monteville Formation (Sequence SW2)

We collected 21 samples from very shallow northwest dipping to subhorizontal interbedded limestone and shale exposed in the valley of the Klein Riet River, northeast of Campbell.

Representative sample behaviour during demagnetization is illustrated in Fig. 9. AF pre-treatment and thermal demagnetization below 225 °C removes a PEF component in all samples except for sample G02C7. The ND overprint is also observed, and as in the Boomplaas Formation, unblocks by 380 °C. At higher temperature steps a few samples (14–18) demagnetize along great-circle trajectories back to a direction similar to the present geomagnetic field, i.e., north and up (NU). These samples vary in lithological character, but were all taken from near the top of the short stratigraphic section. Upon heating to 470 °C, samples from near the base of the section demagnetized towards a shallow westerly upward direc-

tion (W–), which in most cases decayed towards the origin. All four components were identified in sample G02C13, in order of removal: PEF, ND, W– and NU.

4.1.3. Reivilo Formation (Sequence CM5)

Twenty samples of dark grey, massive limestone, ranging from barren to slightly mineralized, were collected from the upper benches of the “P24” open pit of the Pering Pb–Zn mine, eastern Griqualand West. Bedding is regionally horizontal, but samples 11–20 originate from within and across a large (~2 m diameter, ~2 m high) domal stromatolite, leading to significant variance in bedding between these samples. As a matter of curiosity we documented bedding attitudes of our samples from this stromatolite, but we expected that even a primary depositional component would disperse if bedding were to be corrected toward horizontal. Indeed, this proved true for all observed magnetic components.

Each sample has three well-defined and consistent components (see Fig. 10(a)). From NRM to about 225–250 °C, a direction similar to the present-day geomagnetic field (PEF) is interpreted as a VRM with very minor goethite contributions. Weathering in the Pering mine is minimal, but because our samples are from the highest benches of the mine, they could have been affected slightly by weathering.

The second component was removed quite abruptly between 250 and 360 °C (dominantly 300–330 °C), and is directed northward and downward (ND). The unblocking spectrum suggests pyrrhotite as the carrier of this component, and its substantial contribution to the NRM is readily explained by close spatial association of these samples with the Pering sulfide ore body.

The third component, removed between about 400 and 470 °C, is directed westward and shallow-upward (W–). At 480–490 °C, specimen directional behaviour becomes unstable, even though the last stable steps indicate a significant non-zero remainder of the NRM. Trajectories of the stable demagnetization steps above 400 °C either

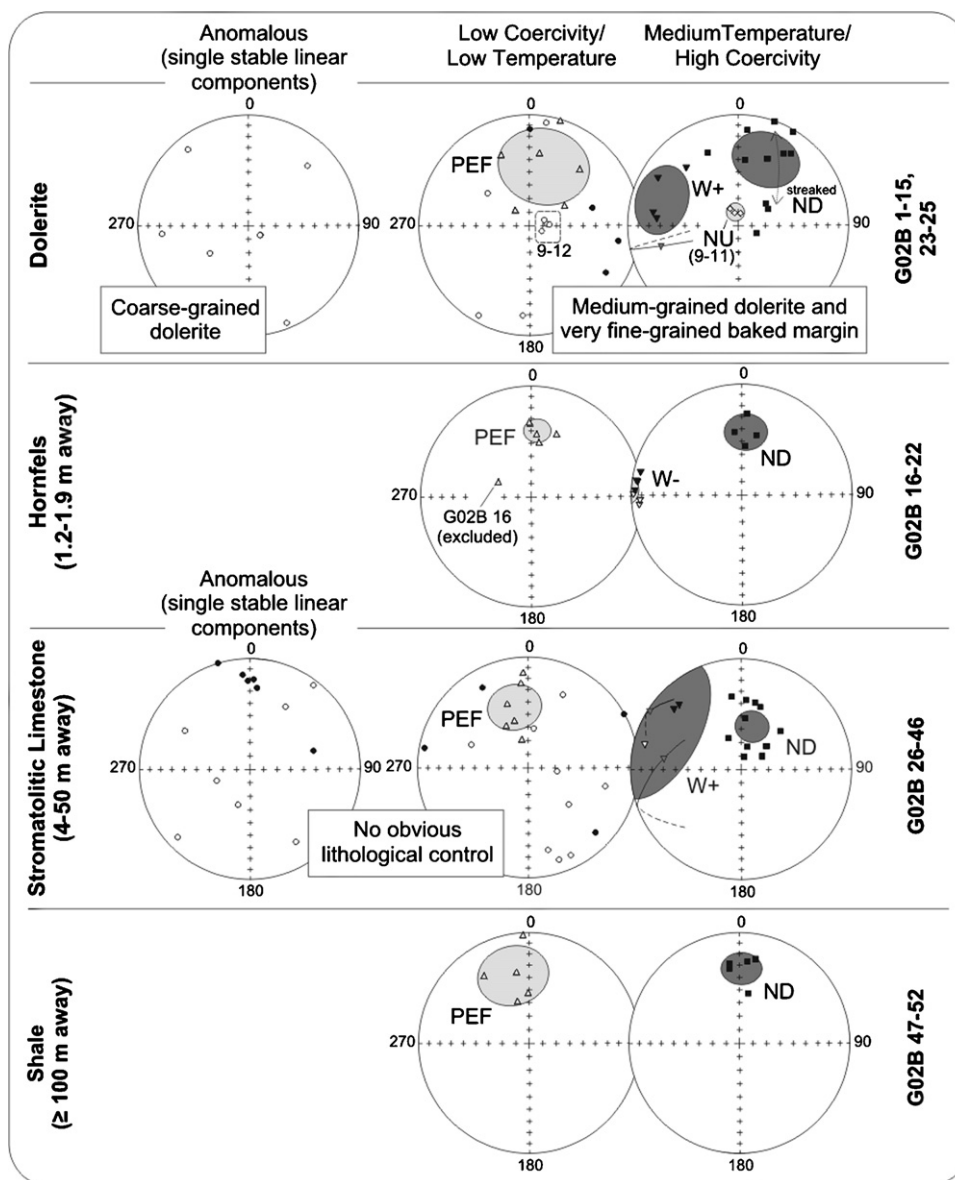


Fig. 8. Results from various lithologies sampled for a baked-contact test at site G02B. Within-site scatter, anomalous magnetic components, and the lack of a stable remanence in country rock render this test inconclusive. Symbols are as in Fig. 5. In addition, diamond symbols show northerly upward directed components (coded NU) believed to represent the present geomagnetic field. These NU components unblock after the north-down directed overprint components at about 360 °C.

point directly toward the origin, or streak toward non-zero values suggesting the presence of an additional component. However, there is no preferred direction to these streaks, and thus they are interpreted as minor spurious laboratory-induced mineral growth with thermo-crystallization remanence.

Calculations of mean directions for each of these three components excluded sample G0CD 18, which was anomalous in all three groupings (Fig. 10(b)). The mean calculation for the third component also excluded sample G0CD 1 (Fig. 10(b)), which was directed significantly apart from the modal group toward the present-field direction, suggesting component mixing. As expected, all three components disperse upon applying a tilt-correction that forces bedding toward horizontal (illustrated in Fig. 10 for the ND and W– components).

4.1.4. Gamohaam Formation (Sequence CM11)

The last outcrop site is located near Kuruman in the northwestern part of the region, where carbonate and banded-iron formation

lithofacies record the conformable passage from subtidal/peritidal environments to deep subtidal during the drowning of the platform (Sumner and Beukes, 2006).

Samples record PEF components, removed at the lowest demagnetization levels, and the regional ND overprint at temperatures characteristic of the Curie temperature of pyrrhotite (Fig. 11). The W+ remanence direction seen in the Boomplaas Formation to the southwest is also present at higher temperature demagnetization levels (Fig. 11). This W+ remanence is conspicuously absent from sites located toward the east (G02D and G02C), where a W– remanence is recorded instead.

4.2. Drill core GKP1

All sample groups, independent of lithology, yielded four magnetic components, with a weakly resolved fifth component (west shallow-down, W+) recorded in some specimens. Typical demagnetization behaviour for carbonate, BIF and tuff samples is illustrated in Fig. 12.

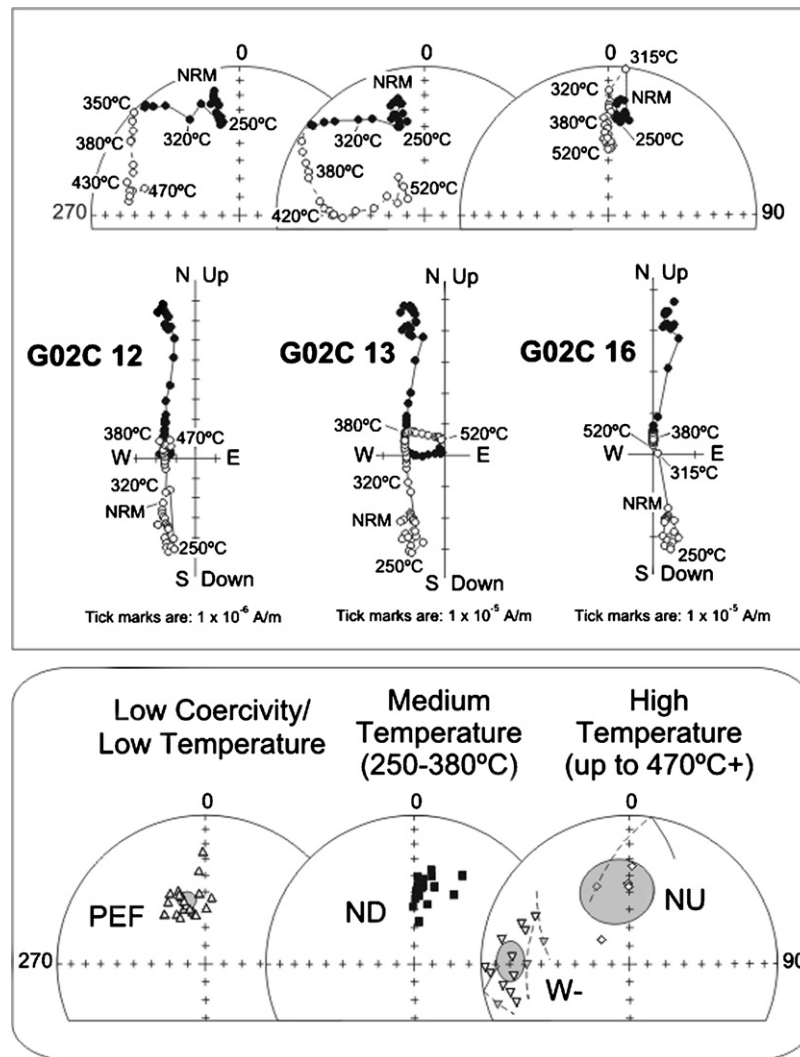


Fig. 9. Demagnetization behaviour and results for shale and carbonate samples from the Monteville Formation in geographic coordinates. Symbols are as in Figs. 4 and 5, and component NU is represented by diamond symbols.

Upon low-field strength AF demagnetization all lithologies from all the sequences sampled revealed remanence components spread about a northeasterly, steep upward direction (referred to here as LOW). Low-temperature (<240 °C) demagnetization then removed scattered magnetizations that were generally directed north to northwest, with negative inclinations of about 55° (coded PEF). Between 240 and 270–300 °C a third component, characterized by clear non-zero seeking linear trajectories on Zijderveld plots, unblocked in nearly all of the samples regardless of lithology or sequence. This intermediate temperature component is directed north and downward at moderate to steep angles (ND).

At higher temperature steps (above 270–300 °C) two magnetic components were revealed. The first of these components is characterized by demagnetization trajectories following great-circle arc paths away from the ND component mean towards scattered near horizontal directions. This fourth component (W+) could only in a few cases be quantified via straight-line fits and was generally only discernable as short segments of great circle arcs away from the ND magnetizations. In most samples, however, demagnetization above 270 °C was characterized by great-circle arc segments away from the ND components towards southerly steep-positive inclination directions (SD), which remained stable up to 470 °C. Above this temperature, sample behaviour became erratic. In the few sam-

ples that recorded the W+ remanence, demagnetization trajectories shift from following a great circle arc away from ND components towards W+ components, to following a great circle arc away from W+ components towards SD components. This switch in trajectory occurs at about 340 °C.

The distributions of all five components are obviously streaked or elongated when plotted (Fig. 13(a)). The causes of streaking in paleomagnetic data can be numerous, as listed by Beck (1999). Sample size effects are a probable cause for the severe streaking of the few W+ directions, but for the remaining four magnetic components (LOW, PEF, ND and SD) our sample populations are sufficiently large ($n > 20$) that the chances of selecting an elongate random sample are very small (Beck, 1999). Incomplete removal of secondary components cannot be wholly ruled out, but seems unlikely because the demagnetization behaviour of most individual samples reveals easily identifiable straight-line segments merging with small or hardly any curvature. Strata intersected by GKP1 dip at shallow angles (usually less than 10°) and no structural disturbance apart from gentle warping can be deduced from the electronic dip-meter log (Fig. 2). For borehole drill core, an additional potential contributor to component streaking is the uncertainty in azimuthal orientation. In some instances multiple “ballmarks” were left on retrieved core due to the rebounding of the core upon breaking or the bumpy journey of the core back to the surface. In such instances the drill over-

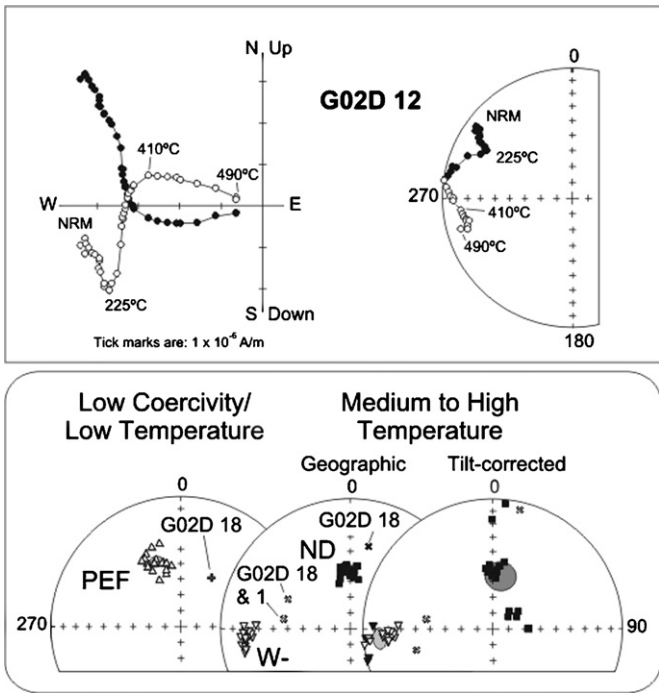


Fig. 10. Demagnetization behaviour from site G02D at the Pb–Zn mine, Pering, in geographic coordinates. The medium and high-temperature components are shown in both geographic and tilt-corrected coordinates. Symbols are the same as previously used. Sample G02D18 displayed inconsistent directions and was excluded for the calculation of component means. The high-temperature component identified from sample G02D1 is suspected of being poorly resolved and component-mixing with the ND component is suspected. It is therefore excluded from the W– mean calculation.

seer selected the best “ballmark” based on bedding surfaces in the retrieved core. Incorrect “ballmark” selection could have resulted in errors in the estimation of the drilling azimuth. Splitting of core is another potential source of errors, as the line along which core is

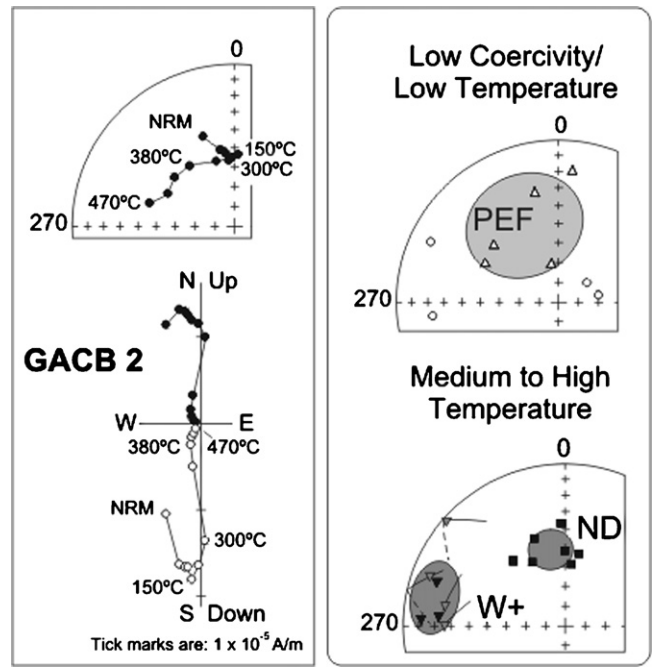


Fig. 11. Demagnetization behaviour from the Gamohaian Formation in geographic coordinates. Symbols are as used before.

split may deviate from the azimuth. These errors should in principle be small, because core recovery was nearly 100% and adjacent ballmarks could be compared for consistency. Furthermore, such errors are equally likely to be either clockwise or anticlockwise away from the true value, thus no systematic error or deflection of the mean are suspected.

The effect of random errors in azimuth estimation can be simulated by rotating a Fisher distributed (Fisher, 1953) dataset by random amounts about an axis that corresponds to the true drilling

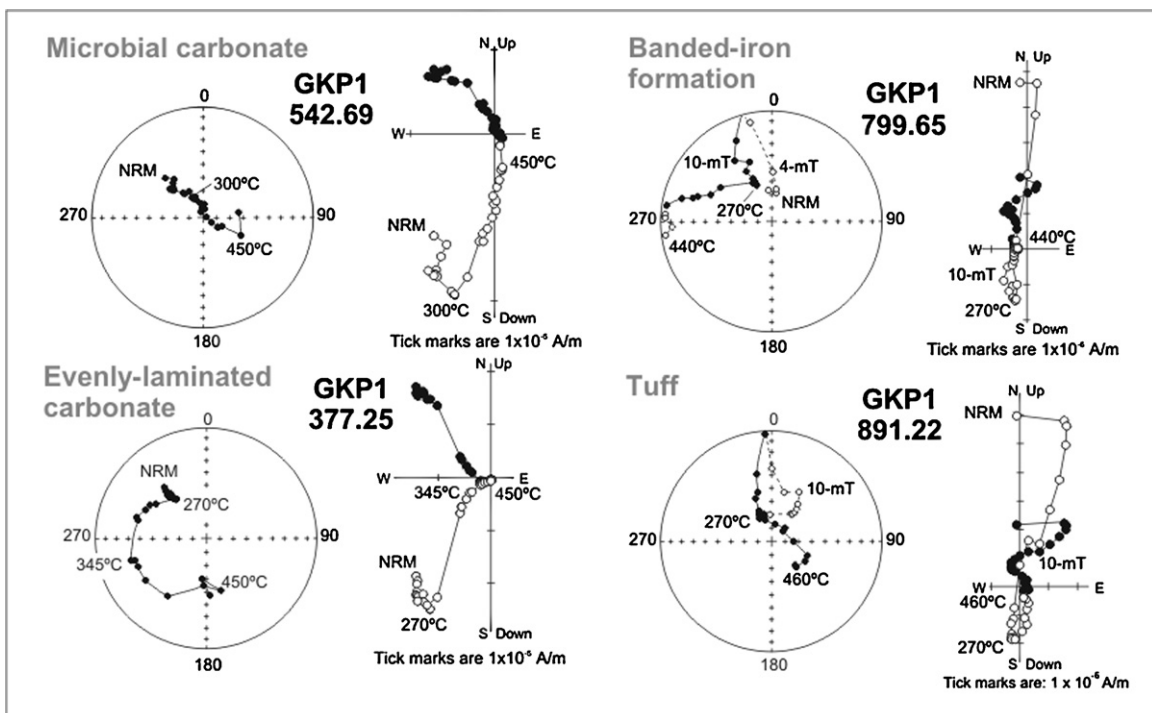


Fig. 12. Representative sample demagnetization behaviour, in geographic coordinates, for microbial carbonate, evenly-laminated carbonate, banded-iron formation and tuff of the Ghaap Group from drill core GKP1. Samples record as many as five magnetic components. Symbols are as in Fig. 4.

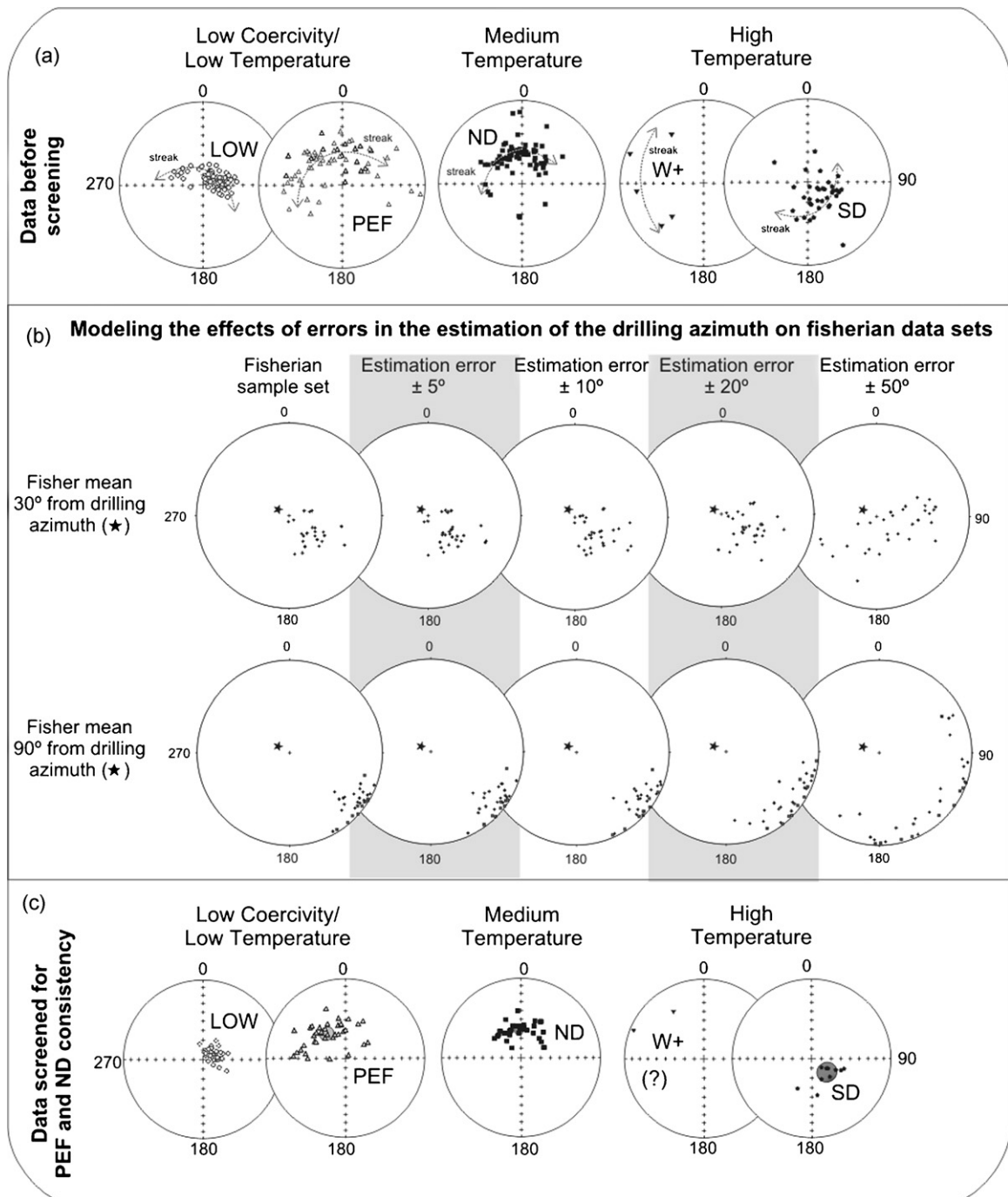


Fig. 13. (a) Equal-area plots of least-squares analyses split into the five identified components for all the lithologies and sequences sampled from core GKP1. Note the pronounced elongated distributions or streaking of all five components. (b) Simulation of the effects of errors, small ($\pm 5^\circ$) to large ($\pm 50^\circ$), in the estimation of the drilling azimuth on the distribution of Fisherian data-sets located close (30°) and far away (90°) from the true drilling azimuth (star). Azimuthal errors as small as 10° have a noticeable effect on distributions. Distortion of data sets becomes more pronounced if the Fisherian sample is further away from the drilling azimuth. (c) Streaking is dramatically reduced if data are screened for PEF and ND-consistency, i.e., the known present geomagnetic field and ND overprints are used as a proxy of how well samples were oriented and how successfully the components were resolved.

azimuth (Fig. 13(b)). Synthetic Fisher-distributed populations of 100 data points each were centred on directions at various angular distances from the drilling azimuth (Fig. 13(b) shows two examples, 30° and 90°). Thirty data points were then randomly selected from each population, and a random rotation, ranging within a specified maximum on either side of the true azimuth (Fig. 13(b) shows four examples, 5° , 10° , 20° and 50°), was applied to each point. These numerical simulations demonstrate that small errors (ca. 10°) in the estimation of the drilling azimuth can result in a noticeable

distortion. The severity of the distortion becomes greater as the angle between the drilling azimuth/rotation axis and the component increases (Fig. 13(b)).

The simulated results closely resemble what is observed in the GKP1 samples (compare Fig. 13(a) and (b)), suggesting that the observed streaking is primarily the result of core azimuthal orientation errors, and that these errors are generally of the order of 20° or smaller. Extremely large ($>20^\circ$) errors in estimation are regarded as unlikely due to the general agreement between the observed

bedding in drill core and that obtained from electronic dip-meter logs.

When calculating component means, only those samples with well defined PEF and ND components similar to those seen in outcrop sites were selected. Both of these components are well defined in outcrop data and shown to be representative of secondary magnetic overprints. They are therefore good proxies with which to assess sample orientation and component isolation. For data screening, samples were treated separately according to lithology. In each lithological group only those samples that record both PEF and ND remanence components were selected, and samples for which PEF or ND line fits had errors of $\geq 15^\circ$ were excluded. However, this still produced distributions with significant streaking. A stricter selection process was attempted by first calculating a mean of the PEF and ND components and then selecting only fits located less than two standard deviations away from the mean. The final selection includes only samples where the PEF and ND components both passed this stricter selection process (Fig. 13(c)), and significantly reduces the amount of streaking, although some of the component distributions are still slightly elongated. Even stricter selection criteria could further reduce elongation, but we believe that the process as outlined above provides a conservative and unbiased estimate of component means.

5. Mean paleomagnetic directions and interpretation of remanence acquisition

5.1. Low-coercivity/low-temperature components (LOW and PEF)

The “softest” magnetic components, removed by low-field AF pre-treatment to 10–15 mT, have either scattered directions (outcrop), are aligned with the present geomagnetic field (PEF), or are directed northwest and upward (borehole, LOW). The PEF component, which in outcrop samples persists up to thermal demagnetization steps of $\leq 250^\circ\text{C}$, is interpreted as a viscous and/or low-temperature crystallization (i.e., weathering) magnetization acquired during the Brunhes polarity epoch. The samples from borehole core GKP1 are unique in this study in that they record a consistent low-coercivity component (LOW) in addition to the PEF magnetization. The LOW component was removed first during demagnetization, and is considered to be related to the drilling process. Drilling induced remanences have long been recognized in paleomagnetic samples taken from drill cores and are often parallel or anti-parallel to the axis of drilling (Jackson and Van der Voo, 1985). The LOW vectors in the GKP01 core are, however, misaligned with the axis of drilling, which was northwesterly ($\sim 310^\circ$) with a $\sim 75^\circ$ dip (Fig. 13). It is possible that the LOW components are the result of mechanical-shock associated with the drilling process (Shi and Tarling, 1999) and not related to the magnetism of the drill-stem. Another interpretation is that the distribution of the LOW remanence is biased towards the PEF direction due to component mixing. A third explanation is that the LOW components are spurious gyromagnetic remanent magnetizations caused by the rotation of the core in the steady field of the drill-stem, but this explanation is considered unlikely since gyroscopic remanent magnetizations are exclusively carried by single-domain grains (Stephenson, 1981) and single-domain grains are not expected to demagnetize at low-AF steps.

5.2. Medium-temperature component (ND)

The north-down component is present throughout the region and is constrained by two intraformational conglomerate tests as being a secondary overprint. The ND component site means combine to yield a total component-mean of declination = 359.2° ,

inclination = 53.8° , $k = 83.7$ and $\alpha_{95} = 5.7^\circ$ (Fig. 14), corresponding to a mean paleomagnetic pole located at 26.5°N , 22.8°E with $A_{95} = 7.0^\circ$. The relatively low and consistent unblocking temperature of ca. 270–380 °C for the ND remanence alludes to pyrrhotite as a possible remanence carrier. Because of the relatively low-Curie temperature ($\sim 320^\circ\text{C}$) of pyrrhotite (Dunlop and Özdemir, 1997) and the abrupt decrease in coercivity as the Curie point is approached, pyrrhotite is easily reset by low-grade thermal events (Clark, 1983; Hanus and Krs, 1968). Paleomagnetic study of pyrrhotite-bearing rocks therefore offers the potential for the detection and the characterization of low-grade thermal events, to which other techniques may be insensitive. The presence of the ND remanence may therefore prove useful in elucidating the tectonic and thermal history of the Transvaal Supergroup strata on the western Kaapvaal craton.

Outcrops of the Transvaal Supergroup have experienced only lower greenschist-facies metamorphism (Button, 1973; Miyano and Beukes, 1984) and the ND remanence should be representative of either the most recent regional thermal event ($>320^\circ\text{C}$) or most recent crystallization event of pyrrhotite. Many possible candidates, like the Mesoproterozoic Namaqua-Natal orogeny or Jurassic Karoo magmatism, can be ruled out by comparing the ND paleomagnetic pole with known directions from the craton (Table 2, Fig. 15). The ND-component pole does, however, bear similarity to the ~ 2.0 and ~ 1.88 Ga pole directions from the Kaapvaal craton (Fig. 15).

The Kaapvaal craton experienced numerous tectono-thermal events at about 2.0 Ga, including intrusion of the Bushveld Complex (Buick et al., 2001) and the Vredefort impact (Kamo et al., 1996). Both of these events have been implicated in the extensive remagnetization seen on the central Kaapvaal craton (e.g., Layer et al., 1988). Extensive intraplate magmatism also occurred during the development of the Waterberg and Soutpansberg rifts at ~ 1.88 Ga (Hanson et al., 2004) and ~ 1.9 Ga (Maier et al., 2003).

Epigenetic Pb–Zn mineralization is present in the Allanridge Formation near the town of Douglas (Whitelaw, 1998), just south of the Boomplaas Formation sites. A 1977 ± 42 Ma Rb/Sr age on chlorite associated with the mineralization and Pb-isotopic age data suggest that it may be linked in space and time (at ~ 2.0 to 1.9 Ga) to other Pb–Zn deposits at Pering and Bushy Park in Griqualand West (Kruger et al., 2001). Gutzmer (2006) attributed the genesis of mineralization at Pering to the rise of metal-bearing fluids from the Ventersdorp Supergroup through to the overlying Transvaal Supergroup. Wholerock Rb/Sr and Pb/Pb ages (Walraven et al., 1991) on Ventersdorp Supergroup volcanics of 1901 ± 83 Ma and $1982 + 169 / - 191$ Ma attest to regional resetting of isotopic systems at about 2.0 Ga. Recent Shrimp U/Pb dating of monazite and xenotime in the Witwatersrand Basin and Transvaal Basin has revealed regionally extensive hydrothermal activity between 2.06 and 2.03 Ga (Rasmussen et al., 2007). Pyrrhotite, the inferred carrier phase of the ND magnetization in all the GKP1 lithologies and outcrop sites, is conspicuously absent from the main mineral assemblage of high-grade ores from the Pering deposit (Gutzmer, 2006). This does, however, not preclude the possibility that pyrrhotite is present as extremely fine-grained particles, which petrographical study has revealed to be present within the lithologies of the Agouron cores (K. Mwamba pers. comm.). The nature and timing of fluids responsible for the Pb–Zn mineralization in the western Kaapvaal craton may therefore allude to the source of the regional 2.0 Ga remagnetization event that characterizes many parts of the Kaapvaal craton.

Kruger et al. (2001) developed a tectonic model for the widespread epigenetic mineralization (see also Duane and Kruger, 1991; Duane et al., 1991) that is essentially a modified version of the one proposed by Oliver (1986) for the expulsion of fluids (responsible for the genesis of Mississippi Valley-type deposits) from thrust

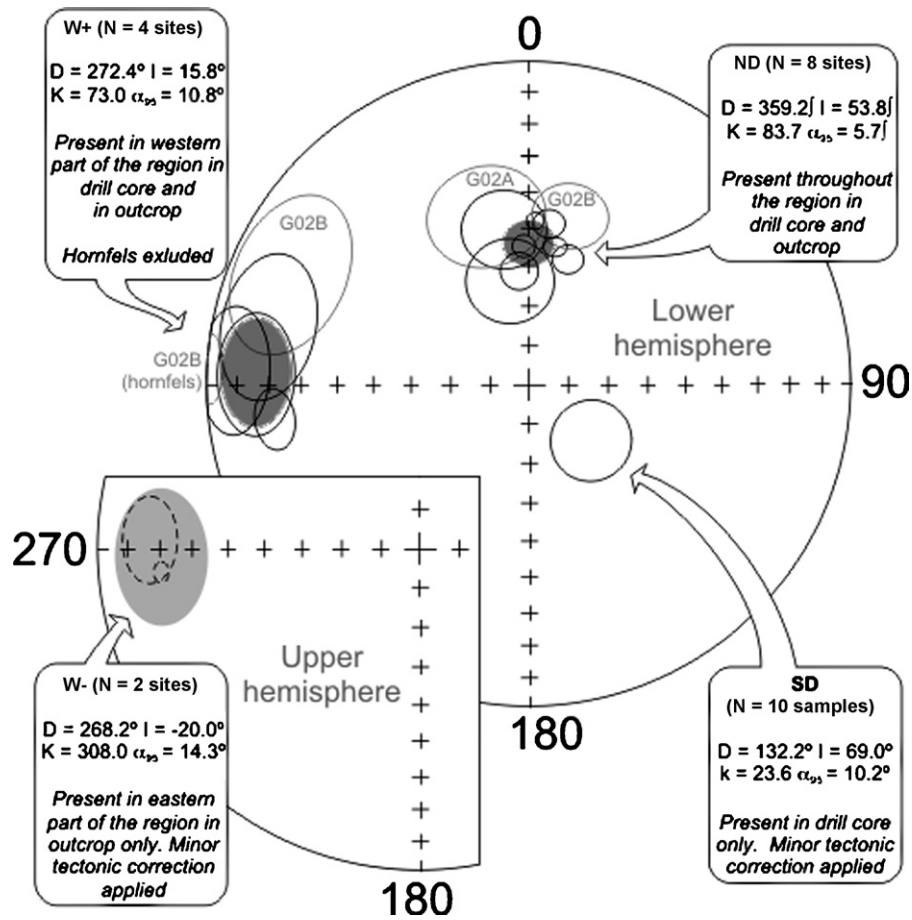


Fig. 14. Summary of site means for the PEF, ND, W+, W- and SD components as identified in outcrop and drill core. Site means with k values smaller than 10 and α_{95} values larger than 15° were excluded from the grand mean calculations. Excluded site means are labeled and drawn in grey. Unfilled ellipses are component means and their associated 95% cones of confidence. Solid ellipse outlines indicate lower hemisphere, stippled ellipse outlines indicate upper hemisphere. Lightly shaded ovals are upper hemisphere and heavily shaded ovals are lower hemisphere.

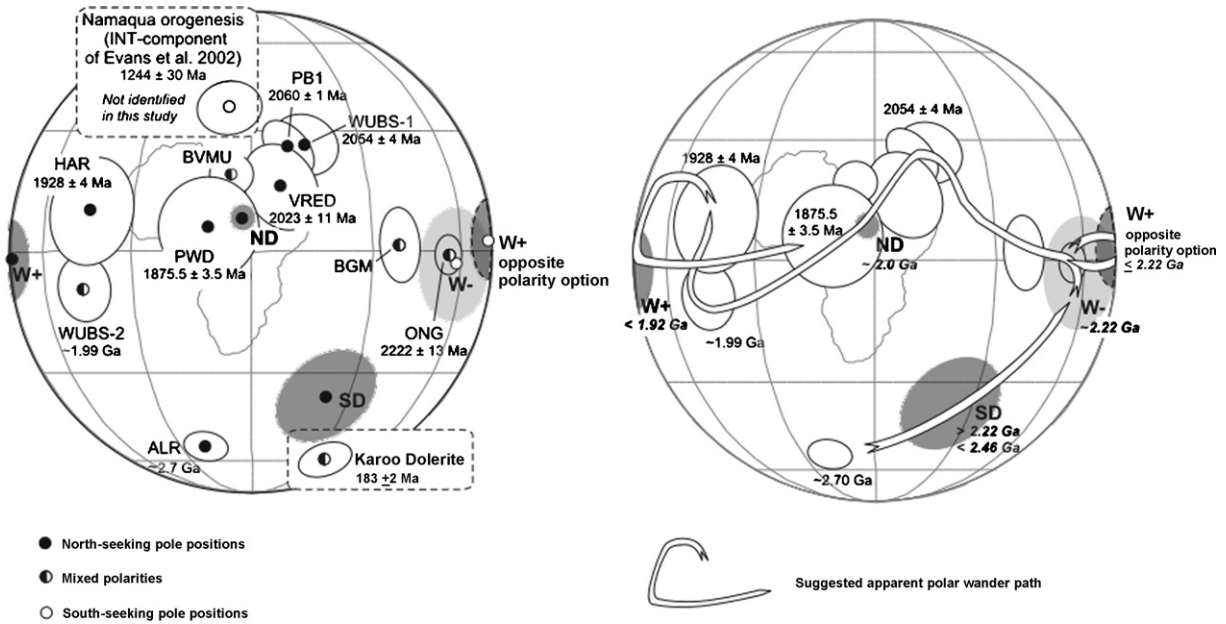


Fig. 15. (a) Comparison of the paleomagnetic poles described by the various components identified in the present study, with known Paleoproterozoic paleopoles from the Kaapvaal craton (Table 2) as well as a Mesoproterozoic overprint direction related to the Namaqua orogenesis and a Jurassic-aged paleopole from Karoo dolerite intrusions. The outline of Africa is merely shown for geographic reference. (b) The swaths show the possible forms of the apparent polar wander path for the Kaapvaal craton in the Paleoproterozoic based on our age assignments for identified components.

Table 2 Mean ancient remanence directions and corresponding paleomagnetic poles from this study and some selected paleopoles from the Kaapvaal craton.

Component	N (number of sites)	Mean declination (deg.)	Mean inclination (deg.)	α_{95}	Latitude °N	k	α_{95}	Longitude °E	dp	dm	K	A ₉₅	Interpreted timing of acquisition	Age Ref.	
ND	8	359.2	53.8	5.7	26.5	83.7	5.7	22.8	6.1	6.1	55.1	7.0	2.0–1.9 Ga	2	
W+	4	272.4	15.8	10.8	-1.8	73.0	10.8	301.5	5.3	5.3	87.7	9.9	Post-1928 Ga or <2.2 Ga	4	
W-	2	268.2	-20.0	14.3	3.2	308.0	14.3	284.1	6.9	10.5	277.7	15.0	~2.2 Ga	5	
SD	1	132.2	69.0	10.2	-48.0	23.6	10.2	65.6	10.9	10.9	dp = 14.7	dim = 17.3	2.5–2.3 Ga	7	
Pole															
Selected paleopoles from the Kaapvaal craton															
Allanridge Fm.					-67.6			355.8	6.1	6.1			~2.7 Ga	1	
Ongeluk Fm.					-0.5			100.7	5.3	5.3			2222 ± 13 Ma	3	
Gamagara/Mapedi Fm. incl. Sishen enriched IF					2.2			81.9	7.2	11.5			2130 ± 92 Ma	5	
Phalaborwa Dykes					35.9			44.8	6.9	10.5			2060.5 ± 0.6 Ma	6	
Waterberg Fm.					36.5			51.3	10.9	10.9			2054 ± 4 Ma	8	
Vredefort impact					22.3			40.7	11.6	15.7			2023 ± 11 Ma	10	
Bushveld Main and Upper Waterberg Fm.					11.5			27.2	4.0	4.0			2061 ± 27 Ma	5	
Hartley Fm.					-10.5			330.4	9.8	9.8			1992 ± 62 Ma	8	
Post-Waterberg dolerite					12.5			332.8	16.0	16.0			1928 ± 4 Ma	5	
					8.6			15.4	17.3	17.3			Recalculated in 8 from 14	14	
INT (Namaqua) overprint					50.6			19.6	9.9	9.9			1244 ± 30 Ma	5	
Karoo dolerite dykes					-68.3			93.7	7.0	7.0			183 ± 2 Ma	16	

References: 1. De Kock (2007); 2. Armstrong et al. (1991); 3. Evans et al. (1997); 4. Cornell et al. (1996); 5. Evans et al. (2002); 6. Morgan and Briden (1981); 7. Reischmann (1995); 8. De Kock et al. (2006); 9. Dorland et al. (2006); 10. Hart et al. (1995); 11. Kamo et al. (1996); 12. Walraven et al. (1998); 13. Cornell et al. (1998); 14. Hanson et al. (2004); 15. Onstott et al. (1986); 16. Hargraves et al. (1997).

sheets associated with Appalachian and Ouachita-orogen tectonics into the interior of the continent. Oliver (1986) assigned key roles to these tectonically driven fluids, including transport of minerals, metamorphism and remagnetization. Protracted hydrothermal activity linked with the Kheis orogen, western Kaapvaal, and the Magondi orogen, western Zimbabwe, are implicated in the model of Kruger et al. (2001).

Deformation in the Magondi orogen (Fig. 16) has a minimum age of 1998 ± 3 Ma, as determined by SHRIMP U–Pb on a cross-cutting granite (McCourt et al., 2001).

Confusion arises because the Kheis province (Fig. 16) was originally defined with geographic boundaries of geophysical and broad tectonic characteristics, namely thin-skinned deformation of the Olifantshoek Supergroup quartzites verging eastward over the Griqualand West cratonic margin. However, more than one orogeny may be responsible for deformation within the Kheis orogen. The most commonly quoted age for Kheis deformation is ca. 1930–1750 Ma, based respectively on data from the mildly deformed Hartley lavas and the ostensibly post-tectonic Mamatlun dolerite (Cornell et al., 1998). However, the Hartley lavas are part of a depositional sequence that rests with regional unconformity upon the beveled folds of Transvaal Supergroup strata that impart the prominent gently undulose map pattern (Fig. 1). Based on regional stratigraphic correlations across semi-continuous exposures of outcrop and boreholes in Griqualand West, southern Botswana, and the Transvaal, Beukes et al. (2002) correlated the Gamagara/Mapedi Formation, which post-date the beveled folds, with Transvaal strata intruded by the 2.06 Ga Bushveld Complex (Fig. 16). At least one phase of folding at the eastern edge of the Kheis province is thus older than 2.06 Ga. The pre-2.06 Ga folds increase in amplitude and decrease in wavelength to the southwest, where they are undoubtedly overprinted by younger structures. Deformation in this southwestern region is as young as ca. 1200 Ma, as indicated by local remagnetization of Transvaal strata immediately adjacent to the Black Ridge Thrust, which lies near, if it does not define, the eastern boundary of the Kheis province (Beukes and Smit, 1987; Evans et al., 2002). Given the abundance of Proterozoic tectonic events affecting this western margin of the Kaapvaal craton, then, we prefer to use the ND pole itself to suggest an age of ca. 2050–2000 Ma for the widespread sulphide-related remagnetization and Pb–Zn ore formation in the Transvaal Supergroup.

Tectonically driven fluid-flow may not be the only explanation for the widespread epigenetic mineralization. Kruger et al. (2001) do mention that the hydrothermal system responsible for the epigenetic mineralization may be related to intrusion of the Bushveld Complex, or events in the Limpopo orogen along the northern margin of the craton. In fact, the close temporal association between the Pb–Zn deposits and the Bushveld Complex has led to a model that proposes a genetic link between them (McClung and Gutzmer, 2004), with emplacement of the complex resulting in localized downward warping and sagging of the craton, reactivating distal basement structures in response to the increased crustal density. Localized hydrothermal convection cells lead to lateral topographically driven fluid migration away from the Bushveld Complex through suitable aquifers such as the Makwassie Formation of the Ventersdorp Supergroup. These fluids, which have by then become metal-rich, rise upwards through reactivated basement structures into the overlying Transvaal Supergroup, and are responsible for the genesis of MVT-type deposits.

The cause of fluid migration, ~2.0 Ga epigenetic mineralization and the remagnetization associated with it is at this stage still obscure, but attractive hypotheses include adjacent crustal thickening in the Kheis or Magondi Orogen and lower crustal heating during the emplacement of the Bushveld Complex.

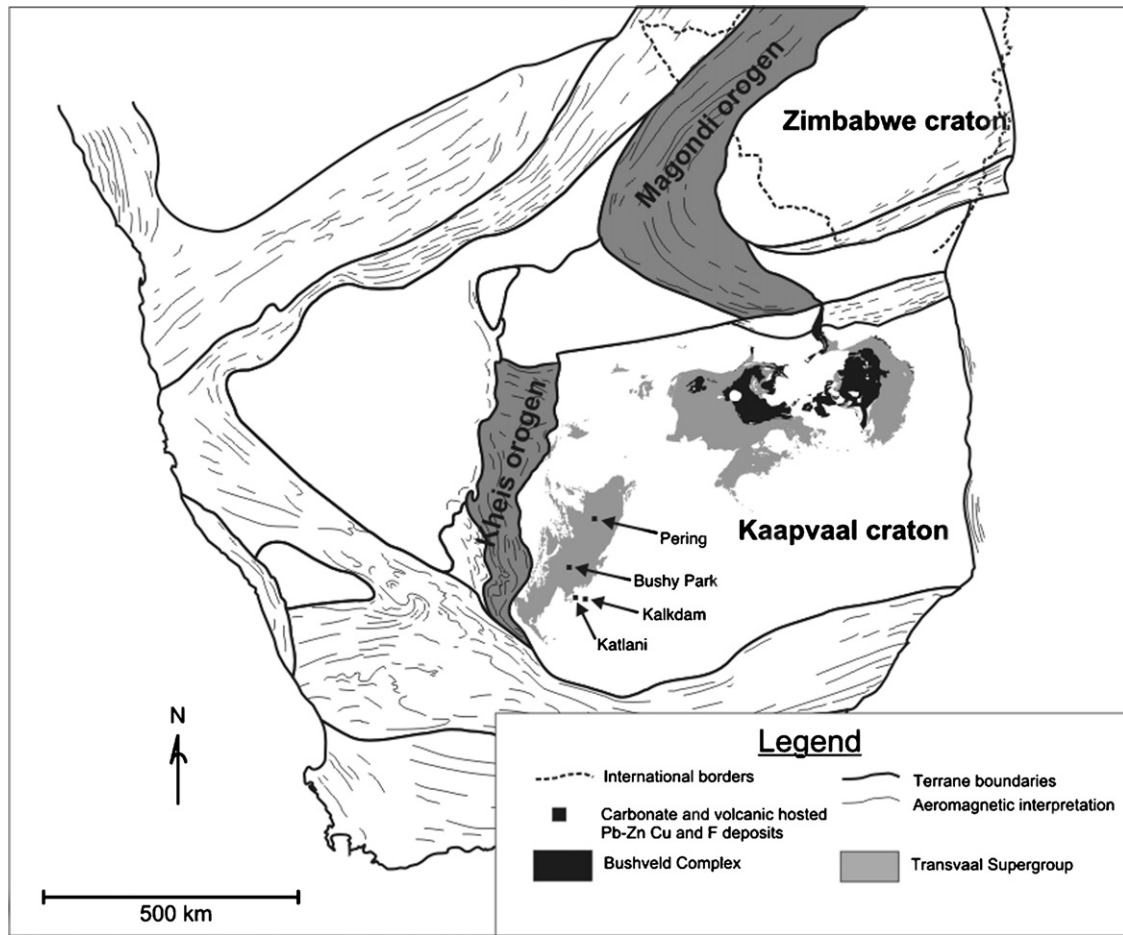


Fig. 16. Tectonic sketch map of southern Africa (based on an aeromagnetic map by De Beers, 1998) showing the Kheis and Magondi orogens, the Bushveld Complex, lower Transvaal Supergroup and epigenetic Pb–Zn deposits.

5.3. High-temperature components

5.3.1. W^+

Shallow west and down (W^+) components dominate sample remanence at higher temperature demagnetization steps at sites near the western margin of the Griqualand West region (i.e., the Boomplaas Formation sites and site GACB). It is also present, rarely, as one of two high-temperature components recorded in drill core GKP1. The W^+ remanence is conspicuously absent in the eastern part of the region. Two intraformational conglomerate tests show the W^+ remanence to be a secondary magnetization. Component means (Fig. 14) combine to yield an average paleomagnetic pole that is located at $-1.8^\circ S$ and $301.5^\circ E$. This pole position (Fig. 15) is similar to, but plots $\sim 30^\circ$ west and $\sim 15^\circ$ south of, the pole from the 1928 ± 4 Ma Hartley Formation (Evans et al., 2002). Alternatively, the W^+ antipole (Fig. 15) shares a likeness with the well-determined 2222 ± 13 Ma Ongeluk Formation paleopole (Cornell et al., 1996; Evans et al., 1997). Either polarity option is permissible, so we turn to the geographical distribution of the W^+ overprint (i.e., limited to the western margin of the Griqualand West region) to explore the likelihood of either option. As discussed above, deformation near the boundary between the Kaapvaal craton and the Kheis province was multi-stage, with events occurring before 2.06 Ga and after 1.93 Ga. The older of these folding episodes deformed strata as young as the Ongeluk lava, which was erosionally bevelled and overlain by Gamagara/Mapedi redbeds that, by correlation, are older than the 2.06 Ga Bushveld Complex. If the W^+ remanence

was acquired during this early event, then the stratigraphic ordering of primary paleomagnetic poles from the Ongeluk and Gamagara/Mapedi units requires a small loop in the APW path to account for the intervening W^+ pole. If, however, the W^+ remanence is related to post-Hartley (post-1928 Ga) deformation of the traditional “Kheis orogeny”, then a ca. 1900–1800 Ma age for the W^+ pole can be inferred. At present we do not have sufficient constraints to distinguish between these alternatives.

5.3.2. W^-

The W^- remanence is limited to sampling sites from the eastern part of the region (Fig. 14), thus suggesting that it is partially or completely overprinted to the west, or that it was not present there at all. This component equates into a pole position that is very similar to the Ongeluk Formation paleopole as well as to a pole from mineralized banded-iron formation below the Gamagara unconformity near Sishen (Fig. 15). The simplest explanation would be that the W^- remanence was acquired as a thermo-chemical remanence during or shortly after the extrusion of the Ongeluk lava. At site G02B, a hornfels-baked zone next to a thick dolerite record a similar W^- (not time-averaged) direction, suggesting that the dyke may be a feeder to the Ongeluk large igneous province that caused the regional (time-averaged) W^- remagnetization. It is suggested that the post-1.93 Ga Kheis tectonism replaced this remanence with the W^+ overprint toward the western part of the region. Our current data, however, do not allow for a field test with which to test this idea.

5.3.3. SD

Drill core revealed a fifth component (SD) that was not identified at any of the outcrop sites (Fig. 14). Whilst this component may prove to be yet another overprint magnetization, the possibility remains that the GKP1 core preserves the primary magnetization of the Ghaap carbonate platform. Although one is easily tempted to proclaim the SD remanence 'primary' and to explain its presence in the core and its absence from outcrops as being related to the immaculate preservation and unaltered nature of the succession intersected by the core, this is not necessarily the case. Some conclusions concerning the age of the SD remanence can be made. It unblocks completely at 470 °C as the last and therefore most stable component of NRM in samples, suggesting magnetite as the magnetic carrier. If the SD component is a chemical remanence, its high stability to thermal demagnetization does not require it to be most ancient. If it is a thermo-chemical remanence associated with processes operating at elevated temperatures above 320 °C, however, then it would be necessarily older than the ND component (i.e., older than ~2.0 Ga), because pyrrhotite, the carrier of the ND remanence, is expected to be sensitive to regional hydrothermal events.

When compared with known poles from the Kaapvaal craton, the SD pole does not resemble any late Paleoproterozoic or Phanerozoic poles from southern Africa. One exception may be the pole from Jurassic dolerite intrusions, which include intrusions in the Griqualand West region, but it plots further to the south, and the dolerite intrusions show dominantly negative inclinations. Thus it is unlikely that the SD remanence is a thermo-chemical remanence younger than 2.2 Ga, but the paucity of the paleomagnetic record from the Kaapvaal craton before 2.2 Ga restricts us from coming to any stronger conclusions. In a recently completed, but as yet unpublished, work (De Kock, 2007) a primary paleomagnetic pole was determined for the ~2.7 Ga Allanridge Formation of the Venterdorp Supergroup. It is interesting to note that the pole for the SD remanence fits snugly between the poles for the Allanridge and the ~2.2 Ga Ongeluk Formation (Fig. 15).

If the SD remanence is primary, it would suggest a constant polarity for the geomagnetic field in a time period of 150–200 Myr, considerably longer than an average geomagnetic superchron (10–100 Myr). Given this, it is much more plausible that the remanence is related to growth of secondary magnetite during burial alteration and metamorphism some time after the deposition of the Kuruman Iron Formation at 2460 ± 5 Ma (Pickard, 2003), but before the extrusion of the Ongeluk lava at 2222 ± 13 Ma (Cornell et al., 1996). The lack of stability field tests makes the age evaluation of the SD component difficult. There is, however, the outside possibility that it represents a much younger remanence, possibly associated with the break-up of Gondwanaland during the Jurassic.

The 52.5° paleolatitude of the Kaapvaal craton, as defined by the SD component acquired after the deposition of the lower Transvaal Supergroup at 2460 ± 5 Ma, contrasts substantially with the low-tropical latitude of Ongeluk lava extrusion at 2222 ± 13 Ma. Minimum rates of pure latitudinal motion ranging from 1.0 to 3.2 cm yr^{-1} can be calculated for the period between the deposition of the lower Asbesheuwel Subgroup and the extrusion of the Ongeluk lava. Estimates vary due to the uncertainties in age and uncertainties in the paleolatitudes of the SD remanence and Ongeluk lava. These estimated rates of movement for the Kaapvaal craton are comparable to modern plate speeds.

6. Conclusions

The strata of the Ghaap Group, which span the Archean-Paleoproterozoic boundary, record a complicated magnetic history reflecting at least 500 million years of the tectono-thermal evo-

lution of the Kaapvaal craton. Five remanence directions were identified. Of these directions, four were readily shown to be secondary magnetizations related to: the present geomagnetic field (PEF), tectono-thermal events affecting the Kaapvaal craton around 1.9–2.0 Ga (ND), Kheis orogeny at either 1.98–1.75 Ga or ca. 2.1 Ga (W+), and emplacement of the Ongeluk large igneous province at 2.222 Ga (W–). The fifth component (SD) was only described from drill core GKP1 and is tentatively suggested to represent burial alteration and metamorphism between 2.46 and 2.42 Ga.

Acknowledgements

We would like to thank the reviewers as well as Chris Rowan, whose comments and suggestions have improved the manuscript considerably. We thank Alec Birch, former geologist at Pering mine, who oversaw drilling of the Agouron drill cores. We also thank Francis Macdonald for his assistance during fieldwork. The management of BHP-Billiton is acknowledged for permission to conduct parts of this investigation at Pering Mine, and we are grateful to the various owners, who allowed us access to their land in the course of this study.

References

- Armstrong, R.A., Compston, W., Retief, E.A., Williams, I.S., Welke, H.J., 1991. Zircon ion microprobe studies bearing on the age and evolution of the Witwatersrand triad. *Precambrian Research* 53, 243–266.
- Barton, J.M.J., Blignaut, E., Salnikova, E.B., Kotov, A.B., 1995. The stratigraphical position of the Buffelsfontein Group based on field relationships and chemical and geochronological data. *South African Journal of Geology* 98, 386–392.
- Beck Jr., M.E., 1999. On the shape of paleomagnetic data sets. *Journal of Geophysical Research* 104 (B11), 25427–25441.
- Beukes, N.J., 1987. Facies relations, depositional environments and diagenesis in a major early Proterozoic stromatolitic carbonate platform to basinal sequence, Campbellrand Subgroup, Transvaal Supergroup, South Africa. *Sedimentary Geology* 54, 1–46.
- Beukes, N.J., Smit, C.A., 1987. New evidence for thrust faulting in Griqualand West, South Africa: implications for stratigraphy and age of red beds. *South African Journal of Geology* 90 (4), 378–394.
- Beukes, N.J., Dorland, H.C., Gutzmer, J., Nedachi, M., Ohmoto, H., 2002. Tropical laterites, life on land, and the history of atmospheric oxygen in the Paleoproterozoic. *Geology* 30 (6), 491–494.
- Buick, I.S., Maas, R., Gibson, R., 2001. Precise U–Pb titanite age constraints on the emplacement of the Bushveld Complex, South Africa. *Journal of the Geological Society, London* 158, 3–6.
- Button, A., 1973. The stratigraphic history of the Malmani dolomite in the eastern and north-eastern Transvaal. *Transactions of the Geological Society of South Africa* 76, 229–247.
- Button, A., 1979. Transvaal and Hamersley Basins—review of basin development and mineral deposits. *Minerals Science and Engineering* 8, 262–290.
- Clark, D.A., 1983. Paleomagnetism of pyrrhotite-bearing rocks. 1438R, CSIRO Restricted Investigation Report. North Ryde, NSW, Australia.
- Cogné, J.P., 2003. PaleoMac: a Macintosh™ application for reconstructions. *Geochemistry Geophysics Geosystems*, 4: pp. 1007, doi:10.1029/2001GC000227.
- Cornell, D.H., Schutte, S.S., Eglinton, B.L., 1996. The Ongeluk basaltic andesite formation in Griqualand West, South Africa: submarine alteration in a 2222 Ma Proterozoic sea. *Precambrian Research* 79, 101–123.
- Cornell, D.H., Armstrong, R.A., Walraven, F., 1998. Geochronology of the Proterozoic Hartley Basalt Formation, South Africa: constraints on the Kheis tectogenesis and the Kaapvaal Craton's earliest Wilson Cycle. *Journal of African Earth Sciences* 26 (1), 5–27.
- De Beers, 1998. Aeromagnetic map. Update on the distribution in time and space of southern African Kimberlites. Produced by Ayers, N.P., Hatton, C.J., Quadling, K.E., Smith, C.D.
- De Kock, M.O., 2007. Paleomagnetism of selected Neoproterozoic-Paleoproterozoic cover sequences on the Kaapvaal craton and implications for Vaalbara. Unpublished PhD Thesis. University of Johannesburg, Johannesburg, 276 pp.
- De Kock, M.O., Evans, D.A.D., Dorland, H.C., Beukes, N.J., Gutzmer, J., 2006. Paleomagnetism of the lower two unconformity-bounded sequences of the Waterberg Group, South Africa: towards a better-defined apparent polar wander path for the Paleoproterozoic Kaapvaal Craton. *South African Journal of Geology* 109 (1), 157–182.
- Dorland, H.C., Beukes, N.J., Gutzmer, J., Evans, D.A.D., Armstrong, R.A., 2006. Precise SHRIMP U–Pb zircon age constraints on the lower Waterberg and Soutpansberg Groups, South Africa. *South African Journal of Geology* 109 (1), 139–156.
- Duane, M.J., Kruger, F.J., 1991. Geochronological evidence for tectonically driven brine migration during the early Proterozoic Kheis orogeny of southern Africa. *Geophysical Research Letters* 18, 957–978.

- Duane, M.J., Kruger, F.J., Roberts, P.J., Smith, C.B., 1991. Pb and Sr isotopes and origin of Proterozoic base metal (fluorite) and gold deposits, Transvaal Sequence, South Africa. *Economic Geology* 86, 1491–1505.
- Duane, M.J., et al., 2004. The timing and isotopic character of regional hydrothermal alteration and associated epigenetic mineralization in the western sector of the Kaapvaal Craton (South Africa). *Journal of African Earth Sciences* 38, 461–476.
- Dunlop, D.J., Özdemir, Ö., 1997. *Rock Magnetism. Fundamentals and Frontiers*. Cambridge University Press, Cambridge, 573 pp.
- Evans, D.A., Beukes, N.J., Kirschvink, J.L., 1997. Low-latitude glaciation in the Palaeoproterozoic era. *Nature* 386, 262–266.
- Evans, D.A.D., Beukes, N.J., Kirschvink, J.L., 2002. Paleomagnetism of a lateritic paleoweathering horizon and overlying Paleoproterozoic red beds from South Africa: implications for the Kaapvaal apparent polar wander path and a confirmation of atmospheric oxygen enrichment. *Journal of Geophysical Research*, 107 (NO. BN12, 2326): doi:10.1029/2001JB000432.
- Fisher, R.A., 1953. Dispersion on a sphere. *Proceedings of the Royal Society of London, Series A* 217, 295–305.
- Greyling, L.N., Huizenga, J.M., Gutzmer, J., 2001. A review of Mississippi Valley-type deposits with emphasis on the Palaeoproterozoic Pering Pb–Zn deposit, South Africa. *Economic Geology Research Institute Information Circular*, 356. University of the Witwatersrand, Johannesburg, 28 pp.
- Gutzmer, J., 2006. The Paleoproterozoic carbonate-hosted Pering Zn–Pb deposit, South Africa. I. Styles of brecciation and mineralization. *Mineralium Deposita* 40, 664–685.
- Hanson, R.E., et al., 2004. Paleoproterozoic intraplate magmatism and basin development on the Kaapvaal Craton: Age, paleomagnetism and geochemistry of ~1.93 to ~1.87 Ga post-Waterberg dolerites. *South African Journal of Geology* 107, 233–254.
- Hanus, V., Krs, M., 1968. Applicability of palaeomagnetism of pyrrhotite to ore-genetic studies. *Mineralium Deposita* 3, 242–248.
- Hargraves, R.B., Rehacek, J., Hooper, P.R., 1997. Paleomagnetism of the Karoo igneous rocks in southern Africa. *South African Journal of Geology* 100 (2), 195–212.
- Hart, R.J., Hargraves, R.B., Andreoli, M.A.G., Tredoux, M., Doucouré, C.M., 1995. Magnetic anomaly near the center of the Vredefort structure: implications for impact-related magnetic signatures. *Geology* 23, 277–280.
- Huizenga, J.M., Gutzmer, J., Banks, D., Greyling, L.N., 2006a. The Paleoproterozoic carbonate-hosted Pering Zn–Pb deposit, South Africa. II. Fluid inclusion, fluid chemistry and stable isotope constraints. *Mineralium Deposita* 40, 686–706.
- Huizenga, J.M., Gutzmer, J., Greyling, L.N., Schaefer, M., 2006b. Carbonic fluid inclusions in Paleoproterozoic carbonate-hosted Zn–Pb deposits in Griqualand West, South Africa. *South African Journal of Geology* 109 (1), 55–62.
- Jackson, M., Van der Voo, R., 1985. Drilling-induced remanence in carbonate rocks: occurrence, stability and grain-size dependence. *Geophysical Journal of the Royal Astronomical Society* 81, 75–87.
- Jones, C.H., 2002. User-driven integrated software lives: “Paleomag” Paleomagnetic analysis on the Macintosh™. *Computers and Geosciences* 28, 1145–1151.
- Kamo, S.L., Reimold, W.U., Krogh, T.E., Colliston, W.P., 1996. A 2.023 Ga age for the Vredefort impact event and a first report of shock metamorphosed zircons in pseudotachylitic breccias and granophyre. *Earth and Planetary Science Letters* 144, 369–387.
- Kirschvink, J.L., 1980. The least squares line and plane and the analysis of palaeomagnetic data. *Geophysical Journal of the Royal Astronomical Society* 62, 699–718.
- Kirschvink, J.L., Kopp, R.E., Raub, T.D., Baumgartner, C.T., Holt, J.W., 2008. Rapid, precise, and high-sensitivity acquisition of paleomagnetic and rock-magnetic data: development of a low-noise automatic sample changing system for superconducting rock magnetometers. *Geochemistry, Geophysics and Geosystems*, 9, Q05Y01, doi:10.1029/2007GC001856.
- Kruger, F.J., Duane, M.J., Turner, A.M., Whitelaw, H.T., Verhagen, B.T., 2001. Palaeohydrology of c. 2 Ga old Mississippi Valley-type Pb–Zn deposits, South Africa: Radiogenic and stable isotopic evidence. *Economic Geology Research Institute Information Circular*, 355. University of the Witwatersrand, Johannesburg, 27 pp.
- Layer, P.W., Kröner, A., McWilliams, M., Clauer, N., 1988. Regional magnetic overprinting of Witwatersrand Supergroup sediments, South Africa. *Journal of Geophysical Research* 93 (B3), 2191–2200.
- Maier, W.D., Peltonen, P., Grantham, G., Mänttari, I., 2003. A new 1.9 Ga age for the Trompsburg intrusion, South Africa. *Earth and Planetary Science Letters* 212, 351–360.
- McClung, C.R., Gutzmer, J., 2004. Fluid flow models in Mississippi-Valley-Type (MVT) deposits: is there only one model? *Geoscience Africa 2004*, Abstract Volume. University of the Witwatersrand, Johannesburg, South Africa, pp. 437.
- McCourt, S., Hilliard, P., Armstrong, R.A., Munyanyiwa, H., 2001. SHRIMP U–Pb zircon geochronology of the Hurungwe granite northwest Zimbabwe: age constraints on the timing of the magondi orogeny and implications for the correlation between the Kheis and Magondi Belts. *South African Journal of Geology* 104, 39–46.
- Miyano, T., Beukes, N.J., 1984. Phase relations of stilpnomelane, ferriannite, and riebeckite in very low-grade metamorphosed iron-formations. *Transactions of the Geological Society of South Africa* 87, 111–124.
- Morgan, G.E., Briden, J.C., 1981. Aspects of Precambrian palaeomagnetism, with new data from the Limpopo Mobile Belt and Kaapvaal Craton in southern Africa. *Physics of the Earth and Planetary Interiors* 24, 142–168.
- Nelson, D.R., Trendall, A.F., Altermann, W., 1999. Chronological correlations between the Pilbara and Kaapvaal Cratons. *Precambrian Research* 97, 165–189.
- Oliver, J., 1986. Fluids expelled tectonically from orogenic belts: their role in hydrocarbon migration and other geologic phenomena. *Geology* 14, 99–102.
- Onstott, T.C., Hargraves, R.B., Joubert, P., Reid, D.L., 1986. Constraints on the tectonic evolution of the Namaqua Province. II. Reconnaissance paleomagnetic and ⁴⁰Ar/³⁹Ar results from the Namaqua Province and Kheis Belt. *Transactions of the Geological Society of South Africa* 89, 143–170.
- Pickard, A., 2003. SHRIMP U–Pb zircon ages for the Palaeoproterozoic Kuruman Iron Formation, Northern Cape Province, South Africa: evidence for simultaneous BIF deposition on Kaapvaal and Pilbara Cratons. *Precambrian Research* 125, 275–315.
- Rasmussen, B., Fletcher, I.R., Muhling, J.R., Mueller, A.G., Hall, G.C., 2007. Bushveld-aged fluid flow, peak metamorphism, and gold mobilization in the Witwatersrand basin, South Africa: constraints from in situ SHRIMP U–Pb dating of monazite and xenotime. *Geology* 35 (10), 931–934.
- Reischmann, T., 1995. Precise U/Pb age determination with baddeleyite (ZrO₂), a case study from the Palaborwa Igneous Complex, South Africa. *South African Journal of Geology* 98, 1–4.
- Schmitz, M.D., Bowring, S.A., 2003. Ultrahigh-temperature metamorphism in the lower crust during Neoproterozoic Ventersdorp rifting and magmatism, Kaapvaal Craton, southern Africa. *Geological Society of America Bulletin* 115 (5), 533–548.
- Schröder, S., Lacassie, J.P., Beukes, N.J., 2006. Stratigraphic and geochemical framework of the Agouron drill cores, Transvaal Supergroup (Neoproterozoic, South Africa). *South African Journal of Geology* 109 (1), 23–54.
- Shi, H., Tarling, D.H., 1999. The origin of bore-core remanences: mechanical-shock-imposed irreversible magnetizations. *Geophysics Journal International* 137, 831–838.
- Stephenson, A., 1981. Gyromagnetic remanence and anisotropy in single-domain particles, rocks, and magnetic recording tape. *Philosophical Magazine B* 44, 635–664.
- Sumner, D.Y., 1997. Carbonate precipitation and oxygen stratification in Late Archean seawater as deduced from facies and stratigraphy of the Gamoha and Frisco Formations, Transvaal Supergroup, South Africa. *American Journal of Science* 297, 455–487.
- Sumner, D.Y., Beukes, N.J., 2006. Sequence stratigraphic development of the Neoproterozoic Transvaal carbonate platform, Kaapvaal Craton, South Africa. *South African Journal of Geology* 109 (1), 11–22.
- Sumner, D.Y., Bowring, S.A., 1996. U–Pb geochronological constraints on deposition of the Campbellrand Subgroup, Transvaal Supergroup, South Africa. *Precambrian Research* 79, 25–35.
- Sumner, D.Y., Grotzinger, J., 2004. Implications for Neoproterozoic ocean chemistry from primary carbonate mineralogy of the Campbellrand-Malmani Platform, South Africa. *Sedimentology* 51, 1273–1299.
- Walraven, F., 1997. Geochronology of the Rooiberg Group, Transvaal Supergroup, South Africa. *Information Circular—University of the Witwatersrand, Economic Geology Research Unit, Johannesburg, South Africa*, 21 pp.
- Walraven, F., Hattingh, P.J., 1993. Geochronology of the Nebo Granite, Bushveld Complex. *South African Journal of Geology* 96, 31–41.
- Walraven, F., Martini, J., 1995. Zircon Pb–evaporation age determinations of the Oak Tree Formation, Chuniespoort Group, Transvaal Sequence: implications for Transvaal-Griqualand West basin correlations. *South African Journal of Geology* 98, 58–67.
- Walraven, F., Armstrong, R.A., Kruger, F.J., 1990. A chronostratigraphic framework for the north-central Kaapvaal craton, the Bushveld Complex and the Vredefort structure. *Tectonophysics* 171, 23–48.
- Walraven, F., Smith, C.B., Kruger, F.J., 1991. Age determinations of the Zoetliet Group—a Ventersdorp Supergroup correlative. *South African Journal of Geology* 94 (2), 220–227.
- Whitelaw, H.T., 1998. Hydrothermal alteration and Pb/Zn mineralization in the Allanridge Formation, Ventersdorp Supergroup, near Douglas, Northern Cape Province, South Africa. Unpublished MSc Thesis. University of the Orange Free State, Bloemfontein, South Africa, 177 pp.